09/754310

Patent Office
Canberra

I, CASSANDRA RICHARDS, ACTING TEAM LEADER EXAMINATION SUPPORT & SALES hereby certify that annexed is a true copy of the Provisional specification in connection with Application No. PQ 4964 for a patent by CANON KABUSHIKI KAISHA filed on 06 January 2000.

WITNESS my hand this
Twelfth day of January 2001

CASSANDRA RICHARDS
ACTING TEAM LEADER
EXAMINATION SUPPORT & SALES

CERTIFIED COPY OF
PRIORITY DOCUMENT

S&F Ref: 461622

ORIGINAL

AUSTRALIA

Patents Act 1990

PROVISIONAL SPECIFICATION FOR THE INVENTION ENTITLED:

Spiral Phase Demodulation for Two Dimensional Fringe Patterns with Circular Carrier Fringes

---

Name and Address of Applicant:

Canon Kabushiki Kaisha, incorporated in Japan, of 30-2, Shimomaruko 3-chome Ohta-ku, Tokyo, 146, Japan

Names of Inventors:

Kieran Gerard Larkin and Michael Alexander Oldfield and Donald James Bone

This invention is best described in the following statement:

SPIRAL PHASE DEMODULATOR FOR TWO-DIMENSIONAL FRINGE PATTERNS

Field of the Invention

The present invention relates to two-dimensional code patterns and more particularly to the automatic demodulation of fringe patterns.

Background

Methods exist for demodulating fringe patterns. However, conventional methods of demodulating closed curve fringe patterns, including circular and elliptical fringe patterns, inevitably produce ambiguities. Ambiguities are then typically resolved by including additional constraints. These additional constraints may include restrictions on the smoothness of curves within the fringe patterns.

In addition to ambiguities other defects and errors may also be produced by the preliminary demodulation process. An example of this can be found in the classic Fourier (Hilbert) transform method (FTM). When the FTM is applied to a whole image, artefacts are produced, the artefacts being related to discontinuities introduced with the half-plane filter used in Fourier space. The artefacts result in errors in phase estimation, and specifically in regions where an angle of the fringe pattern is close to perpendicular with the half-plane discontinuity line.

A method adopted to overcome this problem is to choose the half-plane filter in Fourier space such that the discontinuity line does not cut through the signal in Fourier space.

However, the frequency components derived from circular or elliptical fringe patterns are also "circular" and no discontinuity line could be defined which does not cut through the frequency signal.

Other methods based on local (small kernel) demodulation may avoid the errors of the FTM, but typically fail to disambiguate correctly when there are strong

perturbations in the underlying fringe pattern. Features such as bifurcations and fringe endings represent typically strong perturbations.

Disclosure of the Invention

It is an object of the present invention to substantially overcome, or at least ameliorate, one or more disadvantages of existing arrangements.

According to a first aspect of the invention, there is provided a method of demodulating a real two-dimensional pattern, the method comprising the steps of:

estimating a quadrature two-dimensional pattern from said real two-dimensional pattern using a two-dimensional spiral phase filter; and

creating a demodulated image by combining said real two-dimensional pattern and said estimated quadrature two-dimensional pattern.

According to another aspect of the invention, there is provided an apparatus for implementing the aforementioned method.

According to another aspect of the invention there is provided an apparatus for calculating a quadrature conjugate of a real two-dimensional code pattern, the apparatus comprising:

a first spatial light modulator for modulating coherent light to produce said real two-dimensional pattern;

a first lens for Fourier transformation of said real two-dimensional pattern to produce a first Fourier transformed image;

a second spatial light modulator or spiral phase plate for phase modulating said first Fourier transformed image to produce a phase modulated image;

a second lens for Fourier transformation of said phase modulated image to produce a second Fourier transformed image;

a third spatial light modulator or spiral phase plate for phase modulating said second Fourier transformed image to produce said conjugate of said real two-dimensional pattern; and

an image sensor for capturing said conjugate of said real two-dimensional pattern.

Brief Description of the Drawings

A number of preferred embodiments of the present invention will now be described with reference to the drawings and appendix, in which:

Fig. 1 is an illustration of the local structure of a fringe pattern;

Fig. 2 is an illustration of the Fourier transform of the local fringe pattern of Fig. 1;

Fig. 3A is a flow diagram of a method of phase demodulation;

Fig. 3B is a flow diagram of an alternative method of phase demodulation;

Fig. 4 is an example of a fringe pattern image upon which the preferred embodiment of the invention can be applied;

Figs. 5A and 5B are the real and imaginary parts of an intermediate result in applying the method of Fig. 3B to the image of Fig. 4;

Fig. 6 is an estimate of fringe orientation of the fringe pattern image of Fig. 4;

Figs. 7A and 7B are the magnitude and phase components of a demodulated fringe pattern when the estimate of fringe orientation of the fringe pattern image as shown in Fig. 6 is used;

Fig. 8 is an alternative estimate of fringe orientation of the fringe pattern image of Fig. 4;

Figs. 9A and 9B are the magnitude and phase components of a demodulated fringe pattern when the estimate of fringe orientation of the fringe pattern image as shown in Fig. 8 is used;

Fig. 10 is a schematic block diagram of an optical spiral phase demodulator upon which the preferred embodiment of the present invention can be practiced;

Fig. 11 is a schematic block diagram of a general purpose computer upon which an alternative embodiment of the present invention can be practised; and

Appendix 1 is a paper by the inventors entitled "Generalised Fringe Pattern Analysis using a Spiral Phase Transformation".

Detailed Description including Best Mode

Consider a two-dimensional fringe pattern with intensity of the fringe pattern as follows:

$$f(x,y) = a(x,y) + b(x,y).\cos[2\pi(u_0\{x-x_0\}+v_0\{y-y_0\})+\psi] \quad (1)$$

Position coordinates (x, y) may be continuous for an analog pattern or discrete for digital patterns. A background level is denoted by *a(x,y)* while an amplitude modulation term is denoted by *b(x,y)*, both assumed to be slowly varying functions. Phase term $\psi(x_0, y_0)$ presents the local offset of the overall phase term in the square brackets [] of equation (1).

Referring to Fig. 1, it is assumed that the frequency components u_o and v_o are slowly varying so that they are effectively constant over the small region of interest, Ω, around (x_0, y_0), making the carrier, a linear function of x and y.

A noise term is omitted from equation (1), but may be present in real fringe patterns due to the occurrence of blurring, non linearities, quantisation errors, smudging, scratches, cuts, dust, etc.

The intensity pattern $f(x, y)$ is (generally) a rapidly varying function of (x, y).

The Fourier transform (FT) of the above fringe pattern region Ω is:

$$\begin{aligned} F_\Omega(u,v) &= \iint_\Omega f(x,y)\exp[-2\pi i(ux+vy)]dxdy \\ &= A_\Omega(u,v)+(B_\Omega(u-u_0,v-v_0)\exp[i\psi]+B_\Omega(u+u_0,v+v_0)\exp[-i\psi])e^{-2\pi i(ux_0+vy_0)} \end{aligned} \quad (2)$$

wherein $i = \sqrt{-1}$

From equation (2) it is clear that the Fourier transform of the fringe pattern has 3 lobe centres, the first being at the origin and another two at (u_0,v_0) and $(-u_0,-v_0)$. The last

two lobe centres are mirror images of each other with regards to the origin. The effect of windowing the fringe pattern over a small region Ω is to blur the otherwise sharp lobes. The central lobe A_Ω, representing the zero frequency components, can be removed, and will therefore be disregarded in the following analysis. Methods that may be used for removal of the zero frequency components include using a suitably matched high pass filter. The remaining spectral lobes are illustrated in Fig. 2.

The local spatial frequency components u_0 and v_0 of the fringe pattern satisfies the following equations:

$$\left.\begin{aligned} u_0^2 + v_0^2 &= \sigma_0^2 \\ \sigma_0 &= \frac{2\pi}{\lambda_0} \\ \tan(\beta_0) &= \frac{v_0}{u_0} \end{aligned}\right\} \qquad (3)$$

wherein β_0 is an angle of the normal to the fringes with the x-axis.

The conventional Fourier transform method (FTM) of fringe analysis is based on the assumption that the angle β_0 is confined to a small range for the entire fringe pattern, typically much less than π radians. However, when considering fringe patterns with circular, elliptical carrier patterns or other closed curves, the angle β_0 covers the entire range from 0 to 2π radians. The FTM would therefore be deficient in solving fringe patterns created with closed curve carriers. The reason for this failure is related to the inability of the FTM to isolate the two (mirrored) lobes of the FT. As noted above, the frequency components derived from closed curve fringe patterns are also "closed curves". Therefore, referring again to equation (2), both the second and third terms will have "closed curve" spectral components, causing a total lobe overlap.

The preferred embodiment of the invention removes directional discontinuities in the Fourier processing of the fringe pattern by smoothly encoding the fringe direction by utilizing a filter with odd (180° rotational) symmetry, but (unlike the FTM) a smooth

transition between adjacent frequencies. Also, the filter used in the preferred embodiment does not alter the strength of different frequency components, and is therefore a unit magnitude or phase only filter.

A (complex) Fourier representation $P(u,v)$ of the filter preferably has the following anti-symmetry qualities:

$$P(u,v)=\exp[i\Psi(u,v)]=-P(-u,-v)=-\exp[i(\Psi(u,v)+\pi)] \tag{4}$$

The preferred parameter chosen has a phase which is set equal to the polar angle:

$$\Psi(u,v) = \phi \tag{5}$$

where

$$\left.\begin{array}{c} u=q\cos(\phi) \\ v=q\sin(\phi) \\ u^2+v^2=q^2 \end{array}\right\} \tag{6}$$

The resulting filter is termed a "spiral phase filter" because the filter phase parameter Ψ increases linearly as the polar angle ϕ increases. The magnitude of the filter is constant (so the filter is a pure phase filter) and the phase has the form of a spiral or helical surface with just one turn. An equivalent form of the filter is simply:

$$P(u,v)=\frac{(u+iv)}{q}=e^{i\phi} \tag{7}$$

The Fourier Transform of the fringe pattern after the central lobe has been removed is as follows:

$$F'_{\Omega}(u,v)=\left(B_{\Omega}(u-u_0,v-v_0)\exp[i\psi]+B_{\Omega}(u+u_0,v+v_0)\exp[-i\psi]\right)e^{-2\pi i(ux_0+vy_0)} \tag{8}$$

Applying the spiral phase filter $P(u,v)$ to equation (8) changes the lobe symmetry to gives:

$$\begin{aligned} G(u,v) &= P(u,v).F'_{\Omega}(u,v) \\ &= (B_{\Omega}(u-u_0, v-v_0)\exp[i\psi]\exp[i\phi] - B_{\Omega}(u+u_0, v+v_0)\exp[-i\psi]\exp[i\phi])e^{-2\pi i(ux_0+vy_0)} \end{aligned} \quad (9)$$

Equation (9) can be inverse transformed, as is shown in equation (10), by implicitly assuming that the polar angle $\phi(u,v) \approx \pm \beta_0$ remains constant over each lobe. This is equivalent to assuming that the lobe subtends a small polar angle, which is a reasonable assumption for typical fringe patterns.

$$\begin{aligned} g(x,y) &= \int_{-\infty}^{\infty}\int_{-\infty}^{\infty} G(u,v)\exp[2\pi i(ux+vy)]dudv \\ &= -i\exp[i\beta_0]\sin[2\pi(u_0\{x-x_0\}+v_0\{y-y_0\})+\psi] \end{aligned} \quad (10)$$

The desired sine component of the local fringe pattern $g(x,y)$ can then be extracted by multiplying $g(x,y)$ with an orientational phase component, $\exp[-i\beta_0]$ as follows:

$$g(x,y).\exp[-i\beta_0] = -i\sin[2\pi(u_0\{x-x_0\}+v_0\{y-y_0\})+\psi] \quad (11)$$

Conceptually the process is repeated for all fringe regions with their corresponding fringe orientation angles β. In practice the procedure can be applied to all regions simultaneously. It is noted that the original (conceptual) windowing is not actually required.

The aforementioned process depends upon the functions $b(x.y)$, $\beta(x,y)$, $\psi(x,y)$, $u_o(x,y)$, $v_o(x,y)$, and $\sigma_o(x,y)$ having suitably slow variation. However, it is found in

practice that the preferred embodiment can be successfully implemented on any fringe patterns with suitably smooth variation in orientation and spacing. For fringe patterns with circular fringes and constant or quadratic (chirp) fringe spacing the preferred embodiment only breaks down near the very center of the fringe pattern due to the assumption of small polar angle subtense failing near the centre.

Equation (11) represents an estimation of the imaginary part of the analytic function (or image) related to the original real fringe pattern. This component is also called the quadrature component or analytic conjugate. By forming a new (complex) output image comprising the original real image and the estimated imaginary image, the phase and magnitude of the resulting complex fringe representation can be obtained as follows:

$$(f - a)+(g \exp\{-i\beta_0\}) \approx b.\exp\{-i[2\pi i(u_0\{x-x_0\}+v_0\{y-y_0\})+\psi]\} \qquad (12)$$

A flowchart showing the phase demodulation process is illustrated in Fig. 3A. The fringe pattern image $f(x,y)$, captured in step 10, typically includes only a real part. The fringe pattern image $f(x,y)$ is transformed in step 20 by applying a 2-dimensional FFT. Because the fringe pattern image $f(x,y)$ is real, the real and imaginary parts of the transform $F(u,v)$ are symmetric and antisymmetric respectively.

The DC component (lobe) of the transform $F(u,v)$ is removed in step 30. In step 40, the spiral phase filter $P(u,v)$ is applied to the high passed filtered transform $F(u,v)$. The inverse Fourier transform is calculated in step 50. This may be performed by again applying a 2-dimensional FFT.

In step 60, an orientational phase filter is applied to the resulting image of step 50. In step 70 the real part is discarded, leaving only the imaginary part, which is then added to the input fringe pattern image $f(x,y)$, in step 80 to produce an output image in step 90.

A flowchart showing an alternative embodiment of the phase demodulation process is illustrated in Fig. 3B and will be explained with reference to an example fringe

pattern. An example of such a two-dimensional fringe pattern is illustrated in Fig. 4 wherein only the real part of the pattern is known.

The fringe pattern image *f(x,y)* is captured in step 210. In the alternative embodiment of the phase demodulation process, steps 20 to 50 of the process in Fig. 3A are replaced by a single convolution step 220. The fringe pattern image *f(x,y)* is preferably convolved with spiral phase function *p(x,y)*, wherein *p(x,y)* is defined as follows:

$$\begin{aligned} p(x,y) &= \int_{-\infty}^{\infty}\int_{-\infty}^{\infty} P(u,v)\exp[2\pi i(ux+vy)]dudv \\ &= \int_{-\infty}^{\infty}\int_{-\infty}^{\infty} \frac{(u+iv)}{\sqrt{u^2+v^2}}\exp[2\pi i(ux+vy)]dudv \end{aligned} \tag{13}$$

$$p(x,y) = \frac{i(x+iy)}{2\pi r^3} = \frac{i}{2\pi r^2}\exp(i\theta) \tag{14}$$

wherein

$$\left.\begin{aligned} x &= r\cos\theta \\ y &= r\sin\theta \end{aligned}\right\} \tag{15}$$

The result after such a convolution on the fringe pattern image *f(x,y)* of Fig. 4 is illustrated in Figs. 5A and 5B showing the real and imaginary parts of *f(x,y)*p(x,y)*.

Referring again to Fig. 3B, in step 230 the orientational phase filter, exp[-iβ] is applied. However, an estimation of the fringe orientation β is needed.

A method of estimating the fringe orientation β is to compute the 2-D energy operator which gives uniform estimates over the fringe pattern image *f(x,y)*. Typical gradient based methods fail to give reliable orientation estimates at the peaks and valleys of the fringes. Such a method is described in the publication "A multi-dimensional energy operator for image processing", SPIE Conference on Visual Communications and Image Processing, Boston, MA, [1992], 177-186, by P. Maragos, A.C. Bouik, and J. F.

Quartieri, the contents of which are incorporated herein by cross reference. The 2-D energy operator is applied to the DC removed fringe pattern image separately in the x and y directions as follows:

$$h(x,y) = f(x,y) - a(x,y) \tag{15}$$

where $h(x,y)$ is the intensity of the fringe pattern with the DC removed. $E_x\{\}$ and $E_y\{\}$ are the x and y energy operators respectively and are defined as folows:

$$E_x\{h(x,y)\} = \left(\frac{\partial h}{\partial x}\right)^2 - h\frac{\partial^2 h}{\partial x^2} \approx (2\pi u_0 b)^2 \tag{16}$$

$$E_y\{h(x,y)\} = \left(\frac{\partial h}{\partial y}\right)^2 - h\frac{\partial^2 h}{\partial y^2} \approx (2\pi v_0 b)^2 \tag{17}$$

The 2-D energy operator can be defined as follows:

$$E_x\{h(x,y)\} + iE_y\{h(x,y)\} \approx (2\pi u_0 b)^2 + i(2\pi v_0 b)^2 = (2\pi q_0 b)^2 \exp(2i\beta_0) \tag{18}$$

An overall ambiguity results, because a fringe pattern oriented at 0° cannot be distinguished from a fringe pattern oriented at 180° unless the overall fringe environment is considered. The ambiguity typically appears as an estimate of twice the orientation phase exp[2iβ]. However, step 230 requires a exp[-iβ] phase factor. A simple square rooting gives ±exp[-iβ], again causing an ambiguity. The variation is with respect to a fixed fringe orientation. In Fig. 6 the estimate of the fringe orientation is shown. As the fringes pattern crosses a threshold orientation at β=±90°, the ambiguity "flips". This can be seen in the phase component of a demodulated phase pattern as is illustrated in Figs 7A and 7B wherein the magnitude and phase components of the result of step 230 is shown. Such an ambiguity is tolerable in certain applications. Note that this ambiguity is

a sharp "flip" of sign, quite unlike the (error inducing) directional artefacts of the FTM demodulated phase.

An alternative method of estimating the fringe orientation β is to use an uniform orientation estimator as in the previous method, but to utilise local environmental constraints (such as topology of smoothly varying fringes) to resolve or unravel the orientational ambiguity. Fig. 8 illustrates a smooth estimate of the fringe orientation $\exp(i\beta)$ derived from $\exp(2i\beta)$. The orientation phase estimate has only one discontinuity line at positions where the phase changes from 360° to 0°. A number of different methods are suitable for resolving the orientational ambiguity. The magnitude and phase components of the result of step 230 using the estimation of the fringe orientation β of Fig. 8 is illustrated in Figs 9A and 9B.

It is noted that an estimate of the orientation can be obtained from the output of step 50 in Fig. 3A or alternatively from the output of step 220 in Fig. 3B. However, additional unravelling will be required to obtain a useable orientation estimate.

In step 240 the real part is discarded, leaving only the imaginary part, which is then added to the input fringe pattern image *f(x,y)*, in step 250 to produce an output image in step 260.

The method of Fig. 3A can be practiced using an optical spiral phase demodulator 300, such as that shown in Fig. 10. The optical spiral phase demodulator 300 is illuminated by coherent light 301. A first spatial light modulator (SLM) 302 modulates the coherent light 301 to produce the input image, which is typically a fringe pattern *f(x,y)*. The fringe pattern *f(x,y)* is Fourier transformed by lens 303. A second SLM 304 or a spiral phase plate performs phase modulation in the image projected on it. The phase modulated image is then Fourier transformed by lens 305 and is projected onto a final SLM 306 or spiral phase plate. The final spiral phase plate 306 retards the coherent optical beam in a manner such that the plate introduces a spiral phase multiplication. An image sensor 307 is in close proximity to the final SLM 306 to detect an output image. The output image will be in quadrature (or analytic conjugate) to the input image. In other words, if a cosine pattern is input, a sine pattern is output.

In the special case where the input image is a circularly symmetric fringe pattern, then the SLM 306 has the simple form of a spiral phase with opposite sign to SLM 304.

The method of Fig. 3A or 3B may alternatively be practiced using a conventional general-purpose computer system 100, such as that shown in Fig. 11 wherein the processes of Fig. 3A or 3B may be implemented as software, such as an application program executing within the computer system 100. In particular, the steps of method of phase demodulation are effected by instructions in the software that are carried out by the computer. The software may be stored in a computer readable medium, including the storage devices described below. The software is loaded into the computer from the computer readable medium, and then executed by the computer. A computer readable medium having such software or computer program recorded on it is a computer program product. The use of the computer program product in the computer preferably effects an advantageous apparatus for demodulating two-dimensional fringe patterns in accordance with the embodiments of the invention.

The computer system 100 comprises a computer module 102, input devices such as a keyboard 110 and mouse 112, output devices including a printer 108 and a display device 104.

The computer module 102 typically includes at least one processor unit 114, a memory unit 118, for example formed from semiconductor random access memory (RAM) and read only memory (ROM), input/output (I/O) interfaces including a video interface 122, and an I/O interface 116 for the keyboard 110 and mouse 112. A storage device 124 is provided and typically includes a hard disk drive 126 and a floppy disk drive 128. A magnetic tape drive (not illustrated) may also be used. A CD-ROM drive 120 is typically provided as a non-volatile source of data. The components 114 to 128 of the computer module 102, typically communicate via an interconnected bus 130 and in a manner which results in a conventional mode of operation of the computer system 100 known to those in the relevant art. Examples of computers on which the embodiments can be practised include IBM-PC's and compatibles, Sun Sparcstations or alike computer systems evolved therefrom.

Typically, the application program of the preferred embodiment is resident on the hard disk drive 126 and read and controlled in its execution by the processor 114. Intermediate storage of the program may be accomplished using the semiconductor memory 118, possibly in concert with the hard disk drive 126. In some instances, the application program may be supplied to the user encoded on a CD-ROM or floppy disk and read via the corresponding drive 120 or 128, or alternatively may be read by the user from a network via a modem device (not illustrated). Still further, the software can also be loaded into the computer system 100 from other computer readable medium including magnetic tape, a ROM or integrated circuit, a magneto-optical disk, a radio or infra-red transmission channel between the computer module 102 and another device, a computer readable card such as a PCMCIA card, and the Internet and Intranets including email transmissions and information recorded on websites and the like. The foregoing is merely exemplary of relevant computer readable mediums. Other computer readable mediums may be practiced without departing from the scope and spirit of the invention.

The methods of Fig. 3A or 3B may alternatively be implemented in dedicated hardware such as one or more integrated circuits performing the functions or sub functions of Figs 3A or 3B. Such dedicated hardware may include graphic processors, digital signal processors, or one or more microprocessors and associated memories.

The foregoing describes only some embodiments of the present invention, and modifications and/or changes can be made thereto without departing from the scope and spirit of the invention, the embodiment being illustrative and not restrictive.

The claims defining the invention are as follows:

1. A method of demodulating a real two-dimensional pattern, the method comprising the steps of:

estimating a quadrature two-dimensional pattern from said real two-dimensional pattern using a two-dimensional spiral phase filter; and

creating a demodulated image by combining said real two-dimensional pattern and said estimated quadrature two-dimensional pattern.

2. A method as claimed in claim 1, wherein said estimating step includes the steps of:

generating a frequency domain signal from said real two-dimensional pattern using a linear transform;

applying said two-dimensional spiral phase filter to at least part of said frequency domain signal to provide a filter signal;

generating a spatial domain pattern from said filtered signal using an inverse of said linear transform; and

extracting from the spatial domain pattern an estimate of said quadrature two-dimensional pattern.

3. A method as claimed in claim 1, wherein said estimating step includes the steps of:

convolving said real two-dimensional pattern with a complex function to provide a convolved spatial domain pattern, said complex function being an inverse Fourier transform of said two-dimensional spiral phase filter; and

extracting from the spatial domain pattern an estimate of said imaginary two-dimensional pattern.

4. A method as claimed in any one of claims 2 to 3, wherein the extracting step further includes determining an approximate orientation angle β of at least one fringe pattern in said spatial domain pattern.

5. Apparatus for demodulating a real two-dimensional pattern, the apparatus comprising:

means for estimating a quadrature two-dimensional pattern from said real two-dimensional pattern using a two-dimensional spiral phase filter; and

means for creating a demodulated image by combining said real two-dimensional pattern and said estimated quadrature two-dimensional pattern.

6. Apparatus as claimed in claim 5, wherein said means for estimating an imaginary two-dimensional pattern includes:

means for generating a frequency domain signal from said real two-dimensional pattern using a linear transform;

means for applying said two-dimensional spiral phase filter to at least part of said frequency domain signal to provide a filter signal;

means for generating a spatial domain pattern from said filtered signal using an inverse of said linear transform; and

means for extracting from the spatial domain pattern an estimate of said quadrature two-dimensional pattern.

7. Apparatus as claimed in claim 5, wherein said means for estimating an imaginary two-dimensional pattern includes:

means for convolving said real two-dimensional pattern with a complex function to provide a convolved spatial domain pattern, said complex function being an inverse Fourier transform of said two-dimensional spiral phase filter; and

means for extracting from the spatial domain pattern an estimate of said imaginary two-dimensional pattern.

8. Apparatus as claimed in claims 6 or 7, wherein the extracting means further includes means for determining an approximate orientation angle β of at least one fringe pattern in said spatial domain pattern.

9. Apparatus for calculating a quadrature conjugate of a real two-dimensional code pattern, the apparatus comprising:

a first spatial light modulator for modulating coherent light to produce said real two-dimensional pattern;

a first lens for Fourier transformation of said real two-dimensional pattern to produce a first Fourier transformed image;

a second spatial light modulator or spiral phase plate for phase modulating said first Fourier transformed image to produce a phase modulated image;

a second lens for Fourier transformation of said phase modulated image to produce a second Fourier transformed image;

a third spatial light modulator or spiral phase plate for phase modulating said second Fourier transformed image to produce said conjugate of said real two-dimensional pattern; and

an image sensor for capturing said conjugate of said real two-dimensional pattern.

10. A method of demodulation a real two-dimensional pattern, said method being substantially as described herein with reference to the accompanying drawings.

11. Apparatus for calculating a conjugate of a real two-dimensional pattern, said apparatus being substantially as described herein with reference to Fig. 10 of the accompanying drawings.

Appendix 1 of specification
"Spiral Phase Demodulator for Two-dimentional Fringe Patterns"

Generalised Fringe Pattern Analysis using a Spiral Phase Transformation

Kieran G. Larkin
Donald J Bone*
Michael A. Oldfield

Canon Information Systems Research Australia Pty Ltd.
*CSIRO Division of Mathematics and Information Sciences

Abstract

We introduce an operator with properties that are consistent with the ideas of quadrature and Hilbert transformation in two-dimensional signals or images. The 2-D quadrature algorithm presented relies on a whole new class of operators we call "spiral phase" or vortex operators, which have intriguing orientational properties yet maintain strictly flat spectral response and scale inavariance. We demonstrate the remarkable analytic properties of our spiral phase transformer when applied to bandlimited images such as fringe patterns and suggest wide applicability for general 2-D Hilbert analysis previously considered difficult or even impossible (eg instantaneous 2-D frequency estimation, isotropic texture analysis/synthesis, automatic calibration of phase-shifted interferograms). The spiral phase transform can be efficiently implemented as a compact convolution kernel or as a Fourier space filter. We note that most previous attempts by engineers and physicists to extend the Hilbert transform to 2-D have failed to attain isotropic performance. Connections between our spiral phase operators and the Cauchy-Riemann equations as well as the Riesz transform of harmonic theory are investigated.

1 Introduction

The concept of analytic (or holomorphic) signal was introduced to communication theory by Gabor in 1947[1] for one dimensional (1-D) signals. An analytic signal can be shown to consist of 2 parts; the real part is the base signal and the imaginary part is the Hilbert transform of the real part. Unfortunately the concept does not naturally extend to 2-D. A number of ad hoc definitions of the 2-D Hilbert transform have been proposed [2-8], all of which have varying degrees of directionality (non-isotropism) associated. Typical definitions have quadrant based symmetry.[9, 10] In multidimensional analysis this extends to orthant symmetry.[11] More recently Havilicek et al[12] have proposed the "analytic image" based on work on 2-D texture analysis and 2-D demodulation of AM-FM modelling of image characteristics. A number of improvements are made therein but the definition is not isotropic, as illustrated in their test images. Another new development is the idea of extending the complex analysis of the Fourier transform to hyper-complex numbers. The concept has been called the "quaternionic (W Hamilton 1865) Fourier transform" by Bulow[13, 14], and it allows an unambiguous definition of the analytic image in 2-D. Unfortunately and surprisingly, perhaps, this definition too has a degree of directionality which is apparent in the demodulated envelope patterns.[13] Interestingly the same idea to use quaternions and even octonions was proposed by Craig in 1996[15]. A number of possible definitions of the multidimensional Hilbert transform are considered therein. The quaternionic approach introduces an additional phases in the definition of the analytic image; a direct consequence of hyper-complex numbers with 3 components.

Research in geophysics has produced a number of possible definitions of the 2-D Hilbert transform over the years.[15-19] The idea of a 2-D signum function necessary for 3-D magnetic field analysis was introduced by Nabighian[17] and later applied by Moon et al.[18] However this definition reflects the underlying aim to estimate vertical field derivative from two horizontal field derivatives, so their definition results in a two component complex vector. Our approach effectively shows how a definition of a complex scalar (not vector) 2-D Hilbert transform can be achieved. One of the possible quaternionic Hilbert transforms considered by Craig[15] is, in fact, the "classical" case of Nabighian's.

A study of research in the pure mathematical subject of Harmonic analysis, in particular singular integrals reveals some interesting parallels. Essentially, the generalisation of the Hilbert transform from 1-dimension to n-dimensions is known as the Riesz transform (named after Marcel Riesz[20]). This may explain some of the confusion in recent years regarding the existence of the Hilbert transform for n dimensions, where $n>1$. In a textbook by Stein[21] the proofs of existence, convergence etc of the Riesz transform are derived (see page 56 especially). The Riesz transform is, in fact, a Calderon-Zygmund singular operator.[22] Calderon and Zygmund investigated the higher dimensional analogues of the conjugate function mapping (or Hilbert transform) in the 1950's. More recently research into the so called "bilinear Hilbert transform" has been stimulated by a conjecture of Calderon's in 1951. However, the bilinear Hilbert transform[23] is actually the 1-D Hilbert transform of a function that can be represented as a convolution of two functions, and so very different to a Hilbert transform in 2-D.

Another connection referred to by Nabighian is the generalisation of the Cauchy-Riemann conditions to higher dimensions.[24] This connection is also explored by Stein[25] alongside the Riesz transforms and the Hilbert transform. Adding to the overall confusion Reich[26] gives a rather different definition of a 2-D Hilbert transform based on the work of Calderon and Zygmund[27].

We will outline the major properties and derivation of the 2-D spiral phase transform in section 2 so that it can be compared with the other transforms such as the Riesz. It should be noted that our derivation of the 2-D Hilbert transform analogue is from a very different perspective, and ultimately our transform is not quite the same beast!

we propose a transform which captures the principal properties of the 1-D Hilbert transform and maintains a kind of isotropy in 2-D, yet can be defined within the structure of complex functions in 2-D, without the need for 2-vectors. As we shall see, a direct consequence of this is that these operators may be implemented in optical systems (using phase filters) as well as conventional complex image processing systems. A simplification of the rigorous transform definition allows an easily calculated 2-D Hilbert transform with simple π phase-wrap anistropy but maintains amplitude isotropy.

In addition we define a new class of complex, isotropic, flat spectrum (pure phase) orientation operators which we utilise in transform implementation. Our inspiration, in part at least, for these operators has been the recent work on spiral phase[28-44] (also known as phase singularities, phase vortices, spiral singularities, spiral dislocations, and residues). These phenomena occur naturally in electromagnetic fields whenever there is a zero in the field intensity and can be characterised by a 2-D complex Taylors (or Laurent) series expansion about the zero point.[45] It transpires that these phase spirals have fascinating propagation properties (refs?) which have been the subject of much investigation (refs). In nonlinear media phase singularities can exhibit soliton behaviour[46]. In the study of fringe patterns, the common structures of ridge bifurcation and ridge termination can be modelled simply by underlying singularities.[47-49] In the important area of 2-D phase unwrapping, spiral phases are at the heart of ambiguous unwrapping related to noise and other distortions[45, 50]. But our real interest here has been the effect of optical elements with spiral phase structure and their effects on EM fields.[29, 51-53] In the classic 2-F optical Fourier transform processor a spiral phase can be considered as a complex operator. This turns out to be a very useful way of considering the properties of the 2-D Hilbert transform – as a complex multiplier (operator) in the Fourier domain. In section ? we will cover some relevant background to the spiral phase operator approach to Hilbert transformation.

The isotropic Hilbert transform opens up new applications in pattern analysis previously considered difficult[54] or impossible.[6, 55] In fringe analysis a number of intractable problems become almost trivial because complicated difficulties in spectral zone selection disappear. Many practitioners in the area of signal processing [10] are constrained by suboptimal definitions of the multi-dimensional Hilbert transform. The spiral phase formalism for the two-dimensional Hilbert transform developed in this paper marks a conceptual change from the incumbent linear signum functions to rotary signum functions. The proposed change is not unlike the *preposterous* idea of the screw propeller in the nineteenth century, a time when the paddle steamer was dominant.

2 Definition of the 1-D Hilbert Transform

According to Ahmed Zayed[56] the Hilbert transform was so named by G.H. Hardy after David Hilbert (1862-1943), who was the first to observe the conjugate functions now known as a Hilbert transform pair[57]. Major contributions to the theory of Hilbert transforms were made by Titchmarsh[58] and Gabor.[1] Following its use in the radar theory of Woodward[59] the applications to communication theory developed.[60-62]

Perhaps the best place to start is Bracewell's[63] definition of the Hilbert transform in 1-D:

$$H\{f(x)\} = \frac{-1}{\pi x} * f(x)$$

Where * represents the convolution operator. By the Fourier convolution theorem:

$$\mathbf{F}\{H\{f(x)\}\} = \mathbf{F}\left\{\frac{-1}{\pi x}\right\} F(u)$$

With the forward and inverse Fourier transforms defined as

$$\mathbf{F}\{f(x)\} = F(u) = \int_{-\infty}^{+\infty} f(x)\exp(-2\pi ux)dx,$$

and

$$\mathbf{F}^{-1}\{F(u)\} = f(x) = \int_{-\infty}^{+\infty} F(u)\exp(+2\pi ux)dx.$$

We find

$$\mathbf{F}\left\{\frac{-1}{\pi x}\right\} = i\,\mathrm{sgn}(u) = \begin{cases} +i, u > 0 \\ 0, u = 0 \\ -i, u < 0 \end{cases}$$

In Fourier space the Hilbert transform is obtained by the operation of multiplying by the sign of the frequency ordinate u: a very simple operation. Hence frequency space operations are often preferred for efficient computation. A crucial property of the Hilbert transform is the spectrally independent (that is for any value of the spectral scale factor μ) 90° phase shift, or quadrature property:

$$\left.\begin{aligned} H\{\sin(\mu x)\} &= \cos(\mu x) \\ H\{\cos(\mu x)\} &= -\sin(\mu x) \end{aligned}\right\}$$

Also $f(x) - iH\{f(x)\}$ is known as the (complex) analytic signal, and can be represented as magnitude and phase:

$$f(x) - iH\{f(x)\} = a(x)e^{-i\psi(x)} = a(x)\cos\psi(x) - ia(x)\sin\psi(x)$$

Again, in Fourier space the situation simply depicted as a function with no negative frequency components:

$$\mathbf{F}\{f(x) - iH\{f(x)\}\} = F(u) + \mathrm{sgn}(u)F(u) = \begin{cases} 0, u < 0 \\ F(u), u = 0 \\ 2F(u), u > 0 \end{cases}$$

The above property was used to great effect in the 1980s to revolutionise the analysis of fringe patterns,[64, 65] especially optical interferograms, which were previously analysed manually. The initial methods relied on purely one-dimensional analysis, repeated line by line for 2-D patterns. However, it was soon discovered[66] that the extension to full 2-D allowed much better discrimination between neighbouring frequency components.
The underlying method for 1-D fringe pattern is as follows:

$$f(x) = a(x) + b(x)\cos(2\pi u_0 x + \phi(x))$$

The complex exponential form is:

$$f(x) = a(x) + \frac{b(x)}{2}\left[\exp(2\pi i u_0 x + i\phi(x)) + \exp(-2\pi i u_0 x - i\phi(x))\right]$$

Fourier transforming the above

$$F(u) = A(u) + \frac{1}{2}\left[C(u-u_0) + C^*(u+u_0)\right]$$

where we define the combined amplitude and phase modulated signal c

$$c(x) = b(x)\exp\left(i\phi(x)\right)$$

and the corresponding bandpass spectrum

$$C(u) = \int_{-\infty}^{+\infty} c(x)\exp\left[-2\pi i u x\right]dx$$

It can be shown that, if $b(x)$ and $\phi(x)$ are slowly varying functions, then their Fourier transforms are spectrally localised. A similar argument applies to $a(x)$. The argument can be made quite rigorous, in terms of constraints upon certain derivatives of the functions. Typical functions and transforms are shown in Fig 1 below:

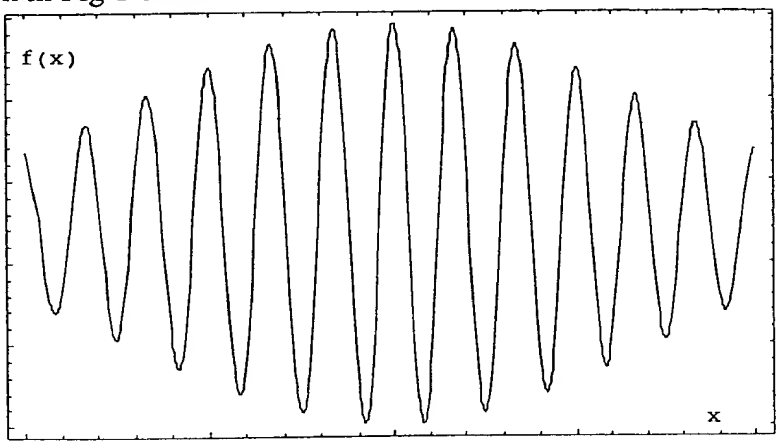

Figure 1(a). Modulated fringe pattern

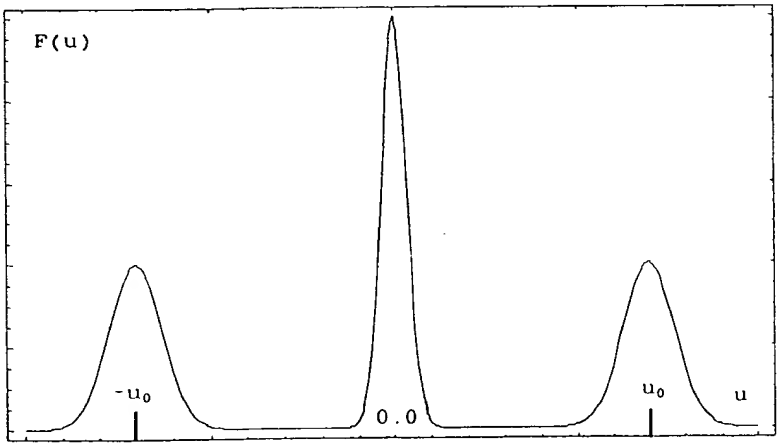

Figure 1(b). Spectrum of modulated fringe pattern

Now it is clear that the Fourier transform (FT) has separated the three components of the original modulated pattern. The FT can be filtered to remove the central (DC) peak and one of the

sidelobes leaving just $C(u-u_0)$, for example. If we now inverse transform the filtered spectrum we get the following:

$$f_{FTM}(x) = \int_{-\infty}^{+\infty} C(u-u_0)\exp[+2\pi i u x]dx = \exp[+2\pi i u_0 x]c(x) = b(x)\exp\left(2\pi i u_0 x + i\phi(x)\right)$$

The next formal step is to find the complex logarithm of the above function:

$$\log\left\{f_{FTM}(x)\right\} = \log\left\{b(x)\right\} + i\left(2\pi u_0 x + \phi(x)\right)$$

In practice the modulus and phase terms are computed as follows:

$$|b(x)| = \sqrt{\left(\Re\left\{f_{FTM}(x)\right\}\right)^2 + \left(\Im\left\{f_{FTM}(x)\right\}\right)^2}$$

$$\mathrm{mod}_{2\pi}\left(2\pi u_0 x + \phi(x)\right) = \arctan\left\{\frac{\Im\left\{f_{FTM}(x)\right\}}{\Re\left\{f_{FTM}(x)\right\}}\right\}$$

We will not consider the further processing of the magnitude and phase information here, but instead will consider the basic transformations that have occurred:

$$f(x) \rightarrow f_{FTM}(x).$$

More specifically

$$b(x)\cos\left(2\pi i u_0 x + i\phi(x)\right) \rightarrow b(x)\left[\cos\left(2\pi i u_0 x + i\phi(x)\right) + i\sin\left(2\pi i u_0 x + i\phi(x)\right)\right]$$

We see that the process essentially involves the generation of a sinusoidal (quadrature) component from a cosine. This is effectively the Hilbert transform of the original fringe pattern, the process is obscured slightly in this instance by the removal of the near-DC component of the signal. The process could be summarised as a short algorithm:

1. Remove DC from signal
2. Fourier transform signal
3. Multiply by signum(frequency)
4. Inverse transform
5. Add this signal (imaginary) to the original function (real and with DC removed)

Typically this is the algorithmic starting point for the extension of the Hilbert transform to 2-D, as we shall see.

3 The 2-D Signum function

Unfortunately the Hilbert transform does not extend naturally into 2-D. Conventional approaches typically involve the definition of a 2-D signum function. The simplest approach has been to define it as a signum operator of one or other of the frequency coordinates:

$S(u,v) = \mathrm{sgn}(u)$

or

$S(u,v) = \mathrm{sgn}(v)$

or more generally

$S(u,v) = \mathrm{sgn}(u')$ where u' is a rotated frequency coordinate.

This simple approach, which is inherently one-dimensional, has been used by a number of researchers.[2, 5, 7, 8, 19, 67] Another common approach has been the alternating quadrant,[3]

$$S(u,v) = \mathrm{sgn}(u)\,\mathrm{sgn}(v)$$

Some researchers have proposed a transform based on a number of alternating sectors[4]

$$S(u,v) = \mathrm{sgn}(\sin(n\phi))$$

where n is an integer and ϕ is the polar angle in frequency space. This type is a generalisation of the preceding definitions. An illustration of the definitions so far is given in Figure 2.

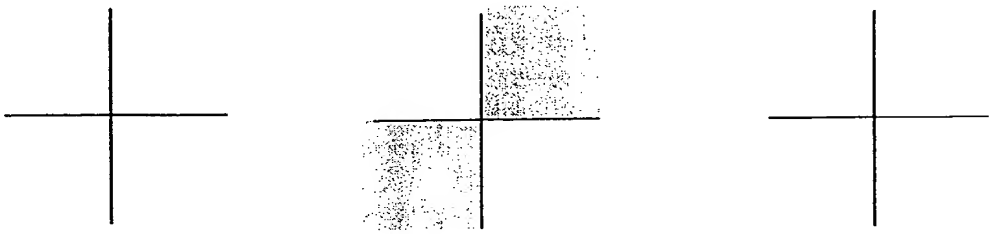

Figure 2. Signum functions for n=1, 2, 3.

The main problem with these definitions is the spatial anistropy and the sharp discontinuity between neighbouring spatial frequencies. A very good way to test for anistropy is to use a test pattern with circular symmetry and apply the candidate Hilbert transform and look for asymmetry in the output. From this point of view all the above candidates fail as Figure 3 shows.

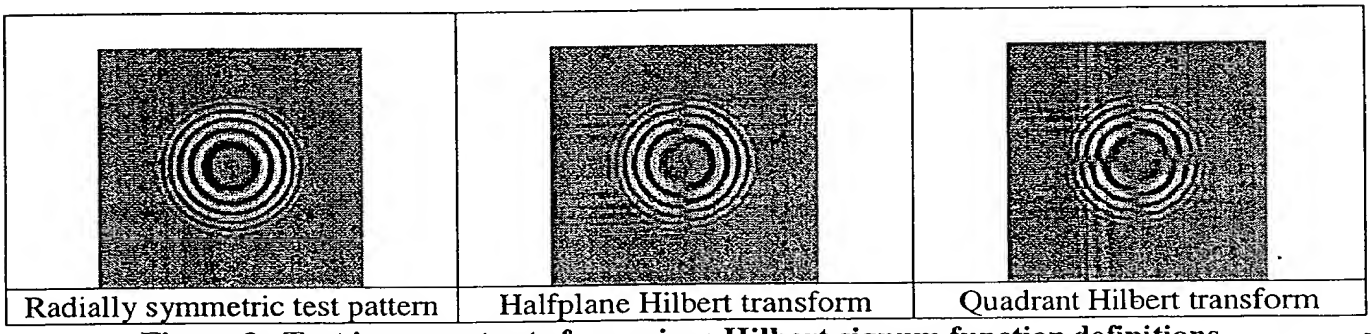

Figure 3. Test image outputs for various Hilbert signum function definitions.

The first pattern in figure 3 is a greyscale representation of a real symmetric function with a chirped frequency and an annular amplitude modulation. The two attempts at 2-D Hilbert transformation show strong direction artefacts. Extending the number of sectors in the signum function merely increases the number of directions, but does not remove the pattern alternation between directions, as the various 2-D quadrant functions proposed by numerous researchers over the years.[3, 9, 11, 68] show.

The 1-D operator ensures that the functional value ant any frequency is the negative of its value at the conjugate frequency (that is to say its 180° rotated frequency). The operator is discontinuous at a single point, the frequency origin. Ideally we would like something in two dimensions which gives a sign change for conjugate frequencies yet avoids discontinuities between neighbouring frequencies. Another property we would (probably) also like to maintain is the non preferential treatment of different frequencies. We can apply these constraints more formally to an idealised 2-D signum function.

$$S(u,v) = -S(-u,-v)$$

and

$$|S(u,v)=1| \Rightarrow S(u,v)=\exp[i\psi(u,v)]$$

imply that

$$\psi(-u,-v)=\psi(u,v)+\pi$$

The constraint upon the neighbouring frequencies is more difficult to state exactly, but it is related to the smoothness of the function and the number and type of discontinuities in S. We will limit our search to the initial problem space of complex functions of two (real) variables u and v, the spatial frequencies. At this point we note that all the recent progress in defining an isotropic Hilbert transform have used either complex vector functions of two real variables[17] or quaternions[13, 15, 17, 18] to allow some extra degrees of freedom in the problem in pursuit of a solution. It is interesting to note that the 2-D Hilbert transform of Nabighian is a complex 2-vector function, and it is not clear how this relates to the original complex scalar function, except when applied to potential function derivatives (in which case a scalar product with a vector gradient produces a scalar!).

Figure 4 defines some important quantities in our problem space

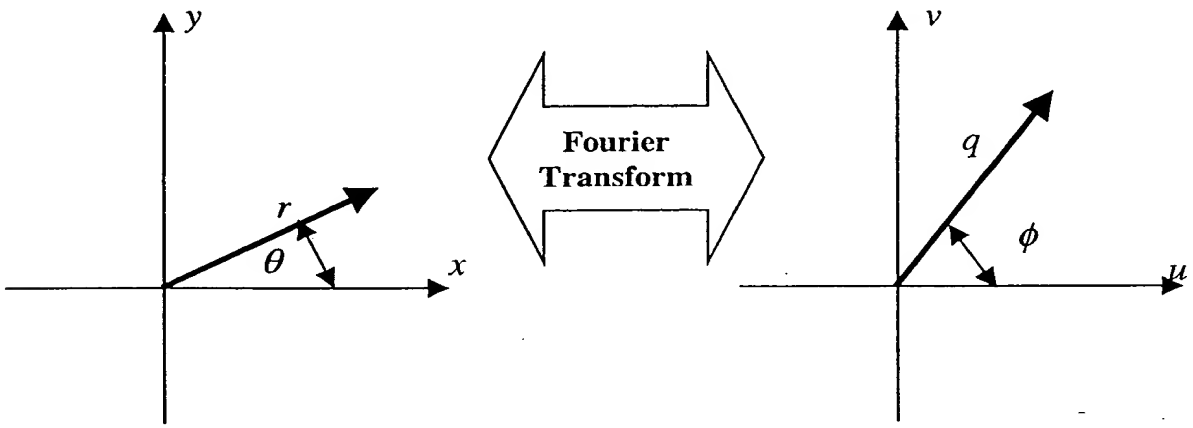

Figure 4. Space and spatial frequency coordinates

Now a possible constraint on S is that is varies uniformly in the radial and tangential spatial frequency coordinates q and ϕ

$$\left|\frac{\partial S}{\partial r}\right| = const$$

and

$$\left|\frac{\partial S}{\partial \phi}\right| = const$$

Nabighian[17] extends a 2-D potential field problem to 3-D and in the process extends what we term a 1-D Hilbert transform to 2-D. The problem he solves seems to naturally extend from 1-D to 2-D, but only with hindsight! He defines a vector Hilbert transform signum function as follows (in our notation):

$$S(u,v) = -\frac{iu}{\sqrt{u^2+v^2}}\mathbf{e}_x - \frac{iv}{\sqrt{u^2+v^2}}\mathbf{e}_y = -i\left(\frac{u}{q}\mathbf{e}_x + \frac{v}{q}\mathbf{e}_y\right)$$

where $\mathbf{e}_x$ and $\mathbf{e}_y$ are unit vectors in the x and y spatial frequency directions (u,v) respectively. Our approach to the problem has been quite different, and perhaps less direct. We propose a signum function as follows:

$$S(u,v) = \exp(i\phi) = \cos\phi + i\sin\phi = \frac{u+iv}{q}$$

Note that the modulus is exactly 1 (except at the origin where it is zero by the Dirichlet condition). Our aim in this instance was to produce a function that is a 1-D signum when evaluated along any radial slice. The radial slice is further "encoded" with a pure phase function that gradually and uniformly varies with the polar angle of the radial slice. The gradual variation is required to avoid the sudden sign changes associated with previous 2-D signum definition when evaluated as radial functions. Our choice gives the following polar derivatives:

$$\frac{\partial S}{\partial r} = 0$$

$$\frac{1}{S}\frac{\partial S}{\partial \phi} = i$$

A few observations about our candidate 2-D signum function are in order at this point. Firstly, the function is not strictly isotropic, but it does have very strong circular symmetric properties. Secondly, the function is what we might call a spiral phase function, or a vortex phase, also known as a spiral discontinuity or (spiral) phase singularity, or a complex residue. The numerous names reflect the importance of this function in many diverse areas of research. From our present perspective the connection between spiral phase and optical diffraction theory, interferometric phase-unwrapping and speckle inteferometry is noteworthy, however we do not have the space (unfortunately!) to explain all the intricate and fascinating interrelations.

We are now about half way through the process of defining an isotropic Hilbert transform – we have a 2-D signum function that fulfils a number of our criteria. But it is no longer possible to define a Hilbert transform purely in terms of real space convolution (frequency space multiplication with a signum function) – an extra operation is required to restore isotropy.

Interestingly, pure mathematicians define an extension of the Hilbert transform to n dimensions which they call the Riesz transform.[21] Just two properties are required to define it: The first is translation invariance, the second is scale invariance. Our definition actually satisfies these constraints because: 1) we have a multiplicative signum function (in the Fourier domain), and 2) our signum is independent of q.

4 Demodulation of 2-D Fringe Patterns

It is useful to consider the stages a test image goes through as we attempt to compute its 2-D Hilbert transform. We will avoid the distinction between continuous and discrete data for the time being to avoid clouding the issue. Figure 5 shows our previously used test function. We have generated an "analytic" image, insofar as we defined a radial symmetric amplitude and a radial symmetric phase function

$$g(x,y) = b(r)\exp[i\phi(r)] = g_R + ig_I$$

We chose a simple, smooth and positive envelope function. The phase consists of a linear function of r. By doing this we already have what we believe to be the exact Hilbert transform of the real part in the imaginary part.

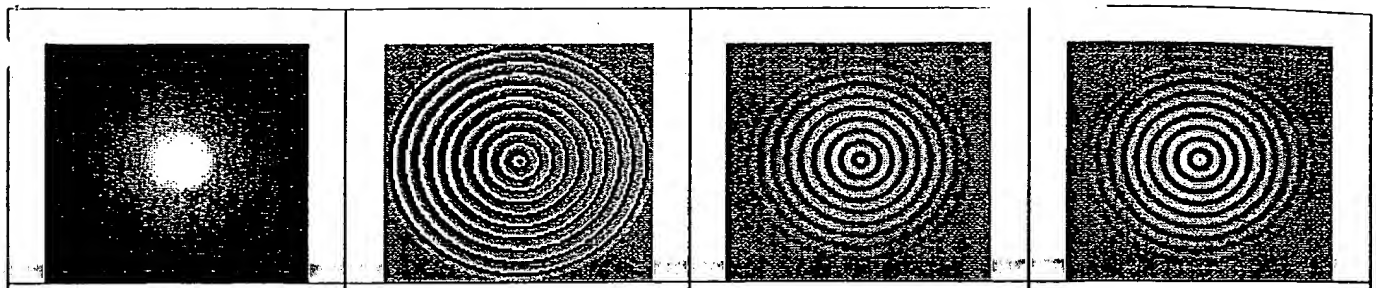

Figure 5.Test function for 2-D Hilbert demodulation tests.

In demodulation problems we can that the cosine component of the signal is known and that the quadrature component is to be estimated. In figure 6 various stages in the Hilbert transform process are shown. Initially (figure 6(a)) the real input function is Fourier transformed, to produce a real symmetric function (by symmetry of FT operation). The Fourier transform shows strong localisation in a ring of frequencies and a ± dipole structure is apparent. A recent paper by Amidor[69] explores the details of such radially periodic functions and their Fourier spectra. The structure if the spiral phase signum function is then shown in terms of real imaginary and phase components. The first stage of our Hilbert transformation is the multiplication of the test image Fourier transform by the spiral phase function. The result of this is shown in terms of its real and imaginary components. In figure 6(b) the product is inverse transformed and displayed as real and imaginary or magnitude and phase components. These two components, expressed as a vector correspond to Nabighian's definition[17] of a 3-D Hilbert transform (given in his equation 22b). Intuitively our expectation of a 2-D Hilbert transform is $H\{g_R\} = -g_I$, or more specifically

$$H\{b(r)\cos[\phi(r)]\} = -b(r)\sin[\phi(r)]$$

We expect an entirely real function with the same (circular in this case) symmetry as the original function. Clearly this is not the case, unless we use the magnitude of the output function (figure 6(b)) $|b(r)\sin[\phi(r)]|$. Using the positive magnitude introduces a feature well known to researchers using FTM – phase ambiguity. Figure 7 shows the theoretical analytic image compared to the analytic image derived from our spiral phase demodulation followed by a magnitude based extraction of the Hilbert component. The phase function looks rather different due to the phase ambiguity. There is also a seeming mismatch in the magnitude of the estimated analytic function. In fact this is likely to be due to the discontinuity in the radial phase function at the origin, and it is not really clear how the analytic function should behave because it can no longer be considered bandlimited.

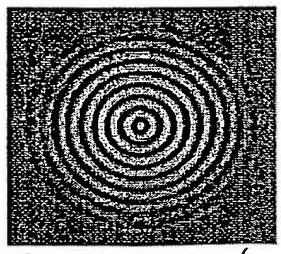

Real test pattern $g_R(x,y)$

Zero imaginary component

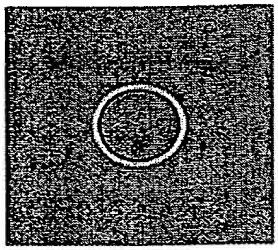

FFT of test pattern (real) $G_R(u,v)$

Zero imaginary component

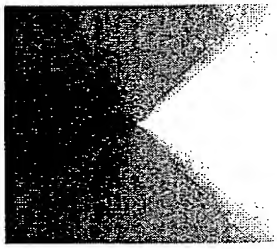

Real part of signum function S(u,v)

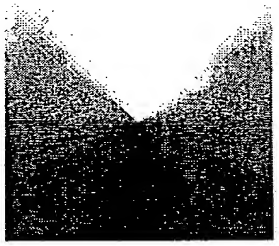

Imaginary part of S(u,v)

Unit magnitude

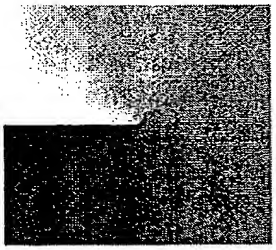

Phase part of S(u,v)

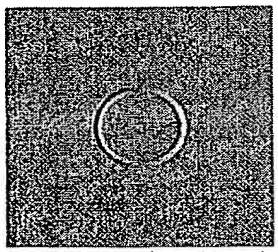

Real part of $S(u,v)G_R(u,v)$

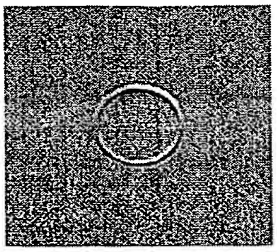

Imaginary part of $S(u,v)G_R(u,v)$

Figure 6(a). Spiral phase signum function operating on test image

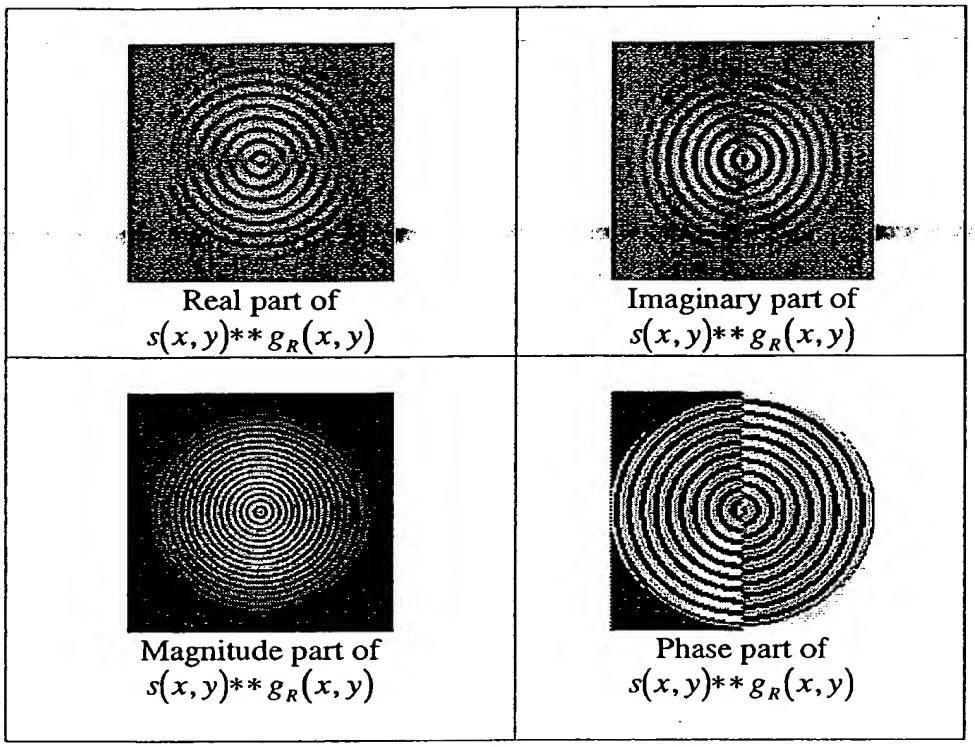

Figure 6(b). Output from spiral phase signum operator

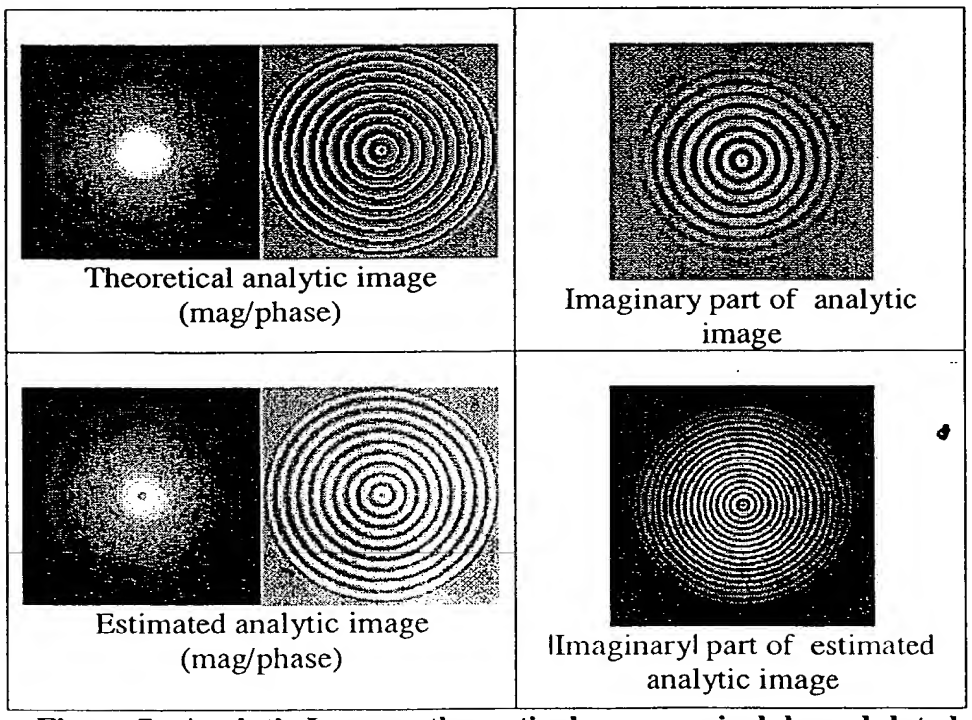

Figure 7. Analytic Images: theoretical versus spiral demodulated

The phase ambiguity appears as a saw tooth profile in the range 0 to π rather than -π to +π as shown in figures 8(a) and 8(b). Mathematically it arises from the arctangent function returning the principal value in the correct quadrant of the full 2π range.

$$\arctan\left[\frac{\sin(\phi)}{\cos(\phi)}\right] = \mathrm{mod}_{2\pi}[\phi+\pi]-\pi$$

$$\arctan\left[\frac{|\sin(\phi)|}{\cos(\phi)}\right] = \begin{cases} \mathrm{mod}_{\pi}[\phi], & \text{if } \mathrm{mod}_{2\pi}[\phi] \le \pi \\ \pi - \mathrm{mod}_{\pi}[\phi], & \text{if } \mathrm{mod}_{2\pi}[\phi] > \pi \end{cases}$$

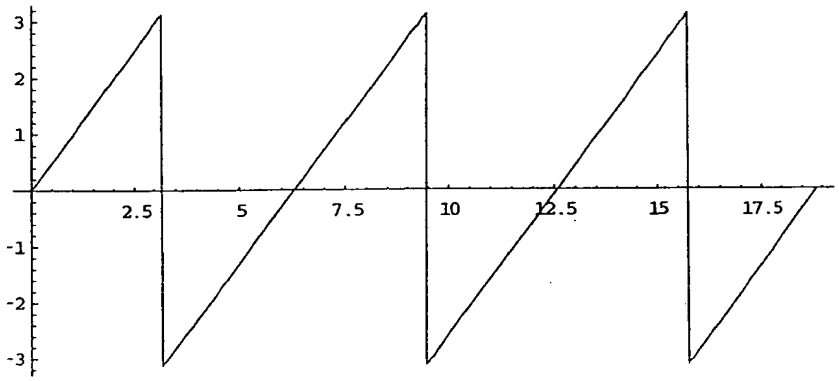

Figure 8(a). Modulo 2π phase calculation

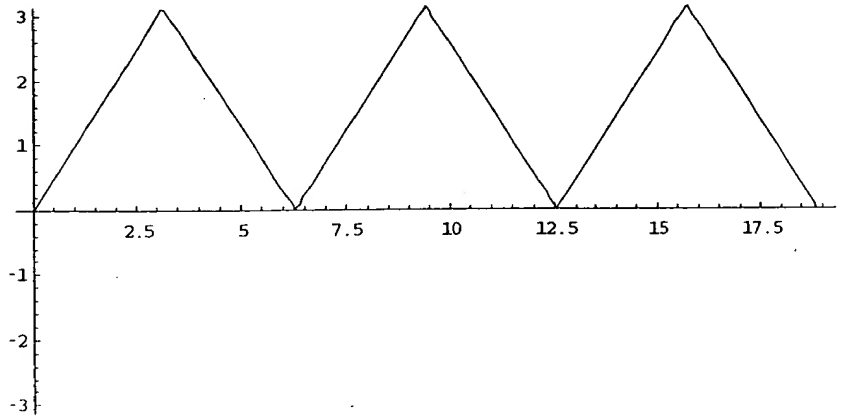

Figure 8(b). Phase calculation with π ambiguity

We shall show later how the phase ambiguity problem may be overcome for many cases of interest.

5 Compensating for the spiral phase encoding

We saw in the previous section how we could define a smoothly varying Fourier space signum function with a spiral phase structure. The simple output from this filter consists of two separate components which do not immediately fit in with our preconceptions of what a 2-D Hilbert transformer should do. To understand more clearly it is helpful to consider a pattern with just one pairs of conjugate frequency components in the Fourier domain. Figure 9(a) shows localised fringe pattern structure that gives rise to significant energy in the sidelobes shown in Figure 9(b).

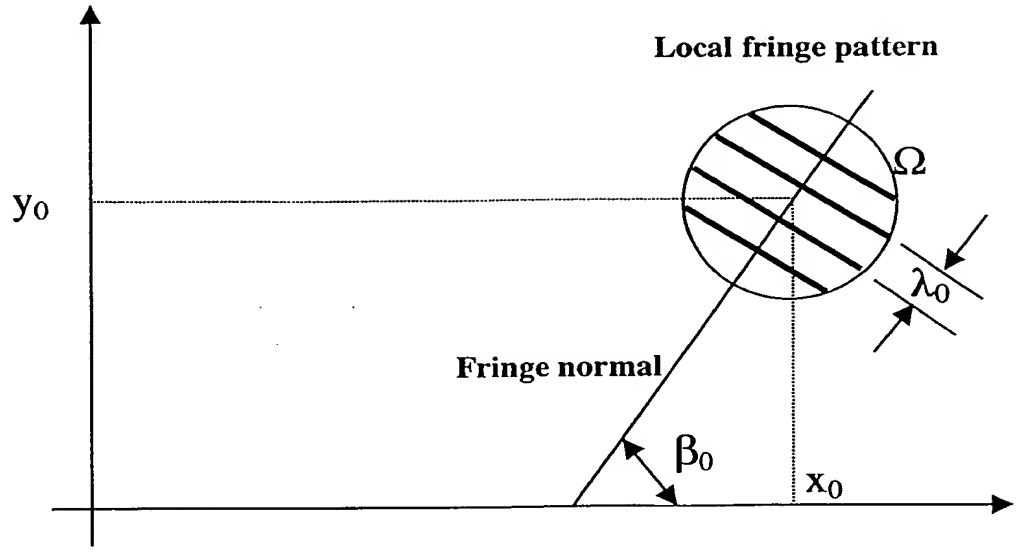

Figure 9(a). Local fringe pattern structure

In Figure 9(a) the 2-D fringe pattern located around coordinates (x_0,y_0) with spatial frequency parameters (u,v) and amplitude b is

$$f(x,y) = a + b\cos\left[2\pi\left(u_0\{x-x_0\} + v_0\{y-y_0\}\right) + \psi\right]$$

Here we assume that the frequency components are slowly varying so that they are effectively constant over the small region of interest, Ω, around (x_0,y_0). The fringe offset and modulation, $a(x,y)$ and $b(x,y)$ are also assumed to be slowly varying functions.
The Fourier transform (FT) of the above fringe pattern region is

$$F_\Omega(u,v) = \iint_\Omega f(x,y)\exp\left[-2\pi i(ux+vy)\right]dxdy$$

$$= A_\Omega(u,v) + B_\Omega(u-u_0, v-v_0)\exp[i\psi] + B_\Omega(u+u_0, v+v_0)\exp[-i\psi]$$

Figure 9(b) shows the sidelobes with the central (near DC) lobe suppressed.

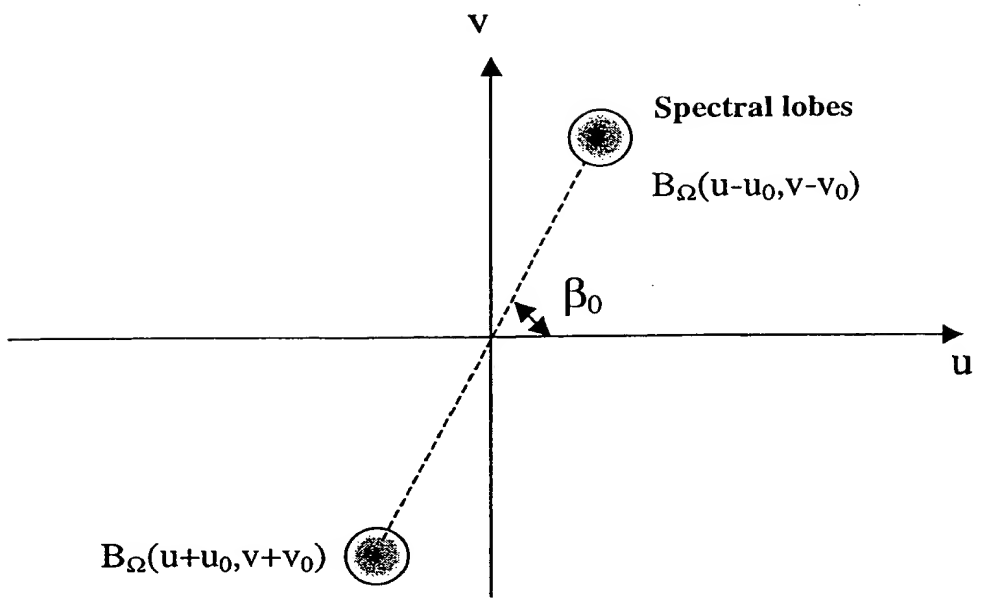

Figure 9(b). Spectral lobes from localised fringe structure

The local spatial frequency of the pattern satisfies the following equations:

$$u_0^2 + v_0^2 = \sigma_0^2$$

$$\sigma_0 = \frac{2\pi}{\lambda_0}$$

$$\tan(\beta_0) = \frac{v_0}{u_0}$$

The normal to the fringes being at an angle β_0 to the x-axis. The conventional Fourier transform method (FTM) of fringe analysis is based on the assumption that the angle β_0 is confined to a small range (certainly much less than π radians). More generally fringe patterns with fringes have the orientation angle β_0 covering the entire range from 0 to 2π radians.
If the 2-D signum function (phase spiral) is applied to the pattern spectrum then we get a sign reversal in the lobes:

$$G(u,v) = \left[F_\Omega(u,v) - A(u,v)\right]\exp[i\psi] = B_\Omega(u-u_0,v-v_0)\exp[+i\psi]\exp[+i\phi] + B_\Omega(u+u_0,v+v_0)\exp[-i\psi]\exp[-i\phi]$$

Now we can transform back (implicitly assuming that $\phi(u,v) \approx \pm\beta_0$ remains constant over each lobe). This is equivalent to assuming that the lobe subtends a small polar angle.

$$g(x,y) = \int_{-\infty}^{+\infty}\int_{-\infty}^{+\infty} G(u,v)\exp\left[2\pi i(ux+vy)\right]dudv$$
$$= -i\exp[i\beta_0]b\sin\left[2\pi i\left(u_0\{x-x_0\} + v_0\{y-y_0\}\right) + \psi\right]$$

So all that remains to be done to recover the sine component of the local fringe pattern is to multiply by $\exp[-i\beta_0]$. The process is repeated for all fringe regions with their corresponding fringe orientation angles β.

$$\exp[-i\beta_0]g(x,y) = -ib\sin\left[2\pi i\left(u_0\{x-x_0\}+v_0\{y-y_0\}\right)+\psi\right]$$

We conjecture that if fringe pattern has suitable constraints upon the smoothness of the fringe parameters (orientation, spacing, offset, and modulation), then the above equation is a good approximation and gives the quadrature component to the original cosinusoidal function.
It was actually shown earlier that the phase function is implicit in the function $g(x,y)$, but with a π phase ambiguity due to the loss of sign information in a square root operation. One way to view this is in terms of the fringes in figure 9(a). If the fringes were rotated 180°, then the diagram would be completely unchanged. However, there are certain constraints upon how fast, and in what way, fringe orientation will vary in many instances. In which case it may be possible to use these constraints to resolve the π ambiguity. As we shall show, it is easier to apply such constraints to the orientation map than it is to apply to the final fringe quadrature estimate. Typically the orientation map $\beta(x,y)$ can be estimated by considering the gradient of the fringe map and extracting the fringe normal. This is similar to the work of Nabighian who computes the z derivative of the field from a scalar product of a 2-D Hilbert transform vector and a gradient vector. In our case this approach can give the same ambiguous results as shown in figure 7 (if we take into account that we are not interested in derivatives of our function, but the functions themselves). It turns out that we can easily overcome the ambiguity by varying degrees by controlling our estimate of $\beta(x,y)$. Firstly it is important to have estimates of $\beta(x,y)$ even when $|\nabla f(x,y)| = 0$, which occurs regularly on the peaks and troughs of the fringes. If these estimates are not available we get very poor results. So we suggest using a method based on 2-D energy operators[70] which include second derivatives and give uniformly distributed estimates of energy and orientation across modulated sinusoids. Other estimates are also possible, but such an investigation would be a major work in itself. We assume a reliable orientation estimator is available. The energy based "gradient" operator we actually use gives estimates of 2β. Using a convenient complex notation we get an estimate of $\exp[2i\beta(x,y)]$ to be precise. Such complex notation is very useful in that it inherently wraps the estimate exactly in line with our inherent (π) ambiguity. In particular, the estimate of β involves first finding the square root of the complex exponential then the argument.

$$\beta = \arg\left\{\pm\sqrt{\exp[2i\beta]}\right\}$$

If we apply the implied algorithm and just take the positive root for simplicity we get a rather nice result for simple closed patterns as is shown in figure 10. Most of the ambiguity induced phase discontinuities are now gone and we have a modulo 2π phase with an overall π "flip" vertically down the centre. For comparison the conventional FTM 1-D Hilbert approach is also shown.

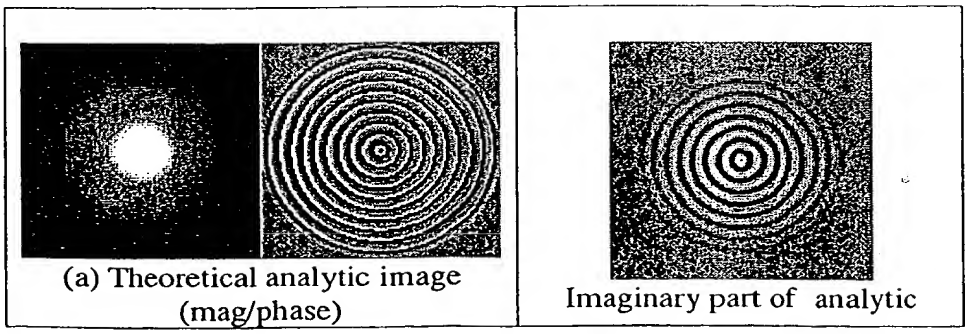

(a) Theoretical analytic image (mag/phase)

Imaginary part of analytic

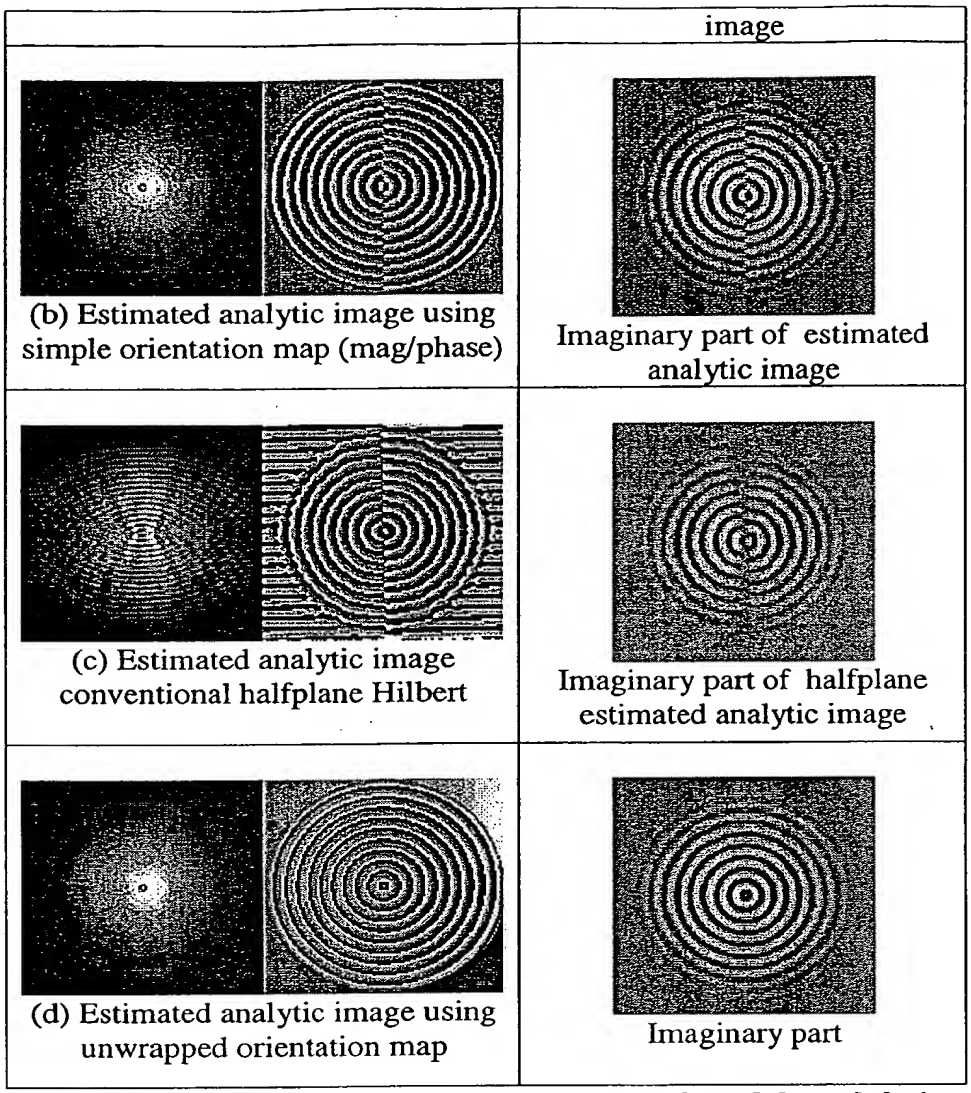

Figure 10. Analytic Images: Orientation map based demodulation.

6 Compensating for ambiguities in the orientation estimator

The estimate of the 2-D Hilbert transformed image in the previous section still has one unwanted feature which is related to an overall ambiguity in the fringe direction resulting in a loss of sign information for our Hilbert transform. There is an elegant solution to this problem which is related to the physical constraints upon the expected fringe pattern structure. If we include a phase unwrapping process with the inherent square root operation on the complex orientation map we can avoid sharp discontinuities in the β estimate due to inappropriate choice of the sign. Essentially we apply an *a priori* restriction on the smoothness of β. There are many ways to do this, but we are fortunate in our approach to the problem because of the strong topological constraints on orientation maps of fringe patterns. Previous work on the analysis of oriented patterns[47-49, 71] used the orientation of the patterns to help extract useful pattern descriptors.

A number of recent works on phase unwrapping have summarised the performance of panoply of algorithm developed in the last few decades. In particular the special processing of phase singularities in phase maps using complex variable analysis (residues etc) has matured. These methods can be used to advantage to unwrap our pure phase orientation map. In our particular case we can have singularities of order +2, +1, -1, whereas conventional interferograms (eg Synthetic Aperture Radar interferograms, speckle interferograms etc) only have +1, and –1, with higher orders being so unlikely as to be virtually non-existent.

We can view our overall process as being optimised to concentrate the unwrapping step (which is needed in ALL existing fringe pattern analysis techniques) in the most easily solved part of the process: the orientation unwrapping. This was not a prior requirement but a natural outcome of our process. The work of Nabighian only really considers functions whose DERIVATIVES obey the Hilbert transform relation. The functions themselves have VECTOR Hilbert transforms in his analysis. We have essentially taken the extra step to reduce the 2 vector Hilbert transform to a real function, in line with our pre-conceptions of what a 2-D Hilbert transform should be.

7 Singular Integrals and the Riesz Transform versus the Quaternionic Hilbert Transform

Subsequent to our discovery and implementation of the spiral phase (vortex) "2-D Hilbert" transformation, our literature searches led to some work on singular integrals by Calderon and Zygmund. It transpires that the second order Riesz transform is analogous to the proposed 2-D Hilbert transform of Nabighian[17] and the first quaternionic transform example by Craig.[15] Stein[21] gives the following example of a n-dimensional Riesz transform in terms of its (n) convolution kernels:

$$K_j(x) = \frac{x_j}{|x|^{n+1}} \quad j = 1 \rightarrow n$$

In terms of the multipliers (viz the Fourier transforms of the kernels):

$$m_j(u) = \frac{u_j}{|u|} \quad j = 1 \rightarrow n$$

So the multiplier effectively defines an n-dimensional signum function, although it is not typically viewed in this way by the pure mathematicians. An important point to note again is that such a transform maps a 2-D real scalar function to a 2-D real vector (2 component) function, whereas are proposal is to map a 2-D real scalar function to a 2-D complex function, then to a 2-D real function (using orientation information). We feel that such an approach is more consistent with our target applications in fringe analysis, image processing and optical diffraction theory, notwithstanding the inevitable difficulties of then extending beyond 2 dimensions. Indeed all proposed operations are possible within the domain of complex operators acting upon complex images.

References

1 D. Gabor, "Theory of communications," Journal of the Institution of Electrical Engineers, **93**, 429-457, (1947).

2 S. Lowenthal, and Y. Belvaux, "Observation of phase objects by optically processed Hilbert transform," Applied Physics Letters **11**, (2), 49-51, (1967).

3 H. Stark, "An extension to the Hilbert transform product theorem," Proceeedings of the IEEE **59**, 13591360, (1971).

4 J. K. T. Eu, and A. W. Lohmann, "Isotropic Hilbert spatial filtering," Optics Communications **9**, (3), 257-262, (1973).

5 J. Ojeda-Castanada, and E. Jara, "Isotropic Hilbert transform by anisotropic spatial filtering," Applied Optics **25**, (22), 4035-4038, (1986).

6 E. Peli, "Hilbert transform pairs mechanisms," Invest. Ophthalmol. Vis. Sci. **30 (ARVO Suppl.)**, 110, (1989).

7 A. W. Lohmann, E. Tepichin, and J. G. Ramirez, "Optical implementation of the fractional Hilbert transform for two-dimensional objects," Applied Optics **36**, (26), 6620-6626, (1997).

8 J. R. Fienup, and C. C. Wackerman, "Phase retrieval stagnation problems and solution," Journal of the Optical Society of America, A **3**, (11), 1897-1907, (1986).

9 Y. M. Zhu, F. Peyrin, and R. Goutte, "The use of a two-dimensional Hilbert transform for Wigner analysis of 2-diemsional real signals," Signal Processing **19**, 205-220, (1990).

10 S. L. Hahn, Hilbert transforms in signal processing, Artech House, Inc., Norwood, MA, 1996.

11 S. L. Hahn, "Multidimensional complex signals with single orthant spectra," Proceeedings of the IEEE **80**, (8), 1287-1300, (1992).

12 J. P. Havlicek, J. W. Havlicek, and A. C. Bovik, "The Analytic Image,," IEEE International Conference on Image Processing, Santa Barbara,California, (1997),

13 T. Bulow, and G. Sommer, " A Novel Approach to the 2D Analytic Signal," CAIP'99, Ljubljana, Slovenia, (1999),

14 T. Bulow, and G. Sommer, "Local Hypercomplex Signal Representations and Applications," Geometric Computing with Clifford Algebra, ed. Sommer, G. Springer Series in Information Sciences, (Berlin: Springer, 1999) Chapter 12.

15 M. Craig, "Analytic Signals For Multivariate Data," Mathematical Geology **28**, (3), 315-329, (1996).

16 M. N. Nabighian, "The analytic signal of two-dimensional magnetic bodies with polygonal cross-section: its properties and use for automated anomaly interpretation," Geophysics **37**, (3), 507-517, (1972).

17 M. N. Nabighian, "Toward a three-dimensional automatic interpretation of potential fiel data via generalized Hilbert transform: fundamental relations," Geophysics **49**, (6), 780-786, (1984).

18 W. M. Moon, A. Ushah, V. Singh, and B. Bruce, "Application of 2-D Hilbert transform in geophysical imaging with potential field data," IEEE Trans Geosci. Remote Sens. **26**, (5), 502-510, (1988).

19 A. E. Barnes, "Theory of 2-D Complex Seismic Trace Analysis," Geophysics **61**, (1), 264-272, (1996).

20 M. Riesz, "Sur les fonctions conjuguees," Mathematische Zeitschrift **27**, 218-244, (1927).

21 E. M. Stein, Singular integrals and differentiability properties of function, Princeton University Press, Princeton, N.J., 1970.

22 A. Carbery, "Harmonic analysis of the Calderon-Zygmund school, 1970-1993," Bulletin of the London mathematical Society **30**, 11-23, (1998).

23 M. T. Lacey, and C. M. Thiele, "On Calderon's conjecture for the bilinear Hilbert transform," Proc. Nat. Acad. Sci. **95**, 4828-4830, (1998).

24 D. G. Fulton, and G. Y. Rainich, "Generalisations to higher dimensions of the Cauchy integral formula," Am. J. Math **54**, 235-241, (1932).

25 E. M. Stein, and G. Weiss, Introduction to Fourier analysis on Euclidean spaces, Princeton Unversity Press, Princeton, N.J., 1971.

26 E. Reich, "Some estimates for the two-dimensional Hilbert transform," Journal D'Analyse Mathematique **XVIII**, 279-293, (1967).

27 A. P. Calderon, and A. Zygmund, "On the existence of certain singular integrals," Acta Mathematica **88**, 85-139, (1952).

28 J. F. Nye, and M. V. Berry, "Dislocations in wave trains," Proc. R. Soc. Lond. A. **336**, 165-190, (1974).

29 W. J. Condell, "Fraunhofer diffraction from a circular annular aperture with helical phase factor," Journal of the Optical Society of America, A **2**, (2), 206-208, (1985).

30 P. Coullet, L. Gil, and F. Rocca, "Optical Vortices," Optics Communications **73**, (5), 403-408, (1989).

31 E. Abramochkin, and V. Volostnikov, "Spiral-Type Beams," Optics Communications **102**, (3-4), 336-350, (1993).

32 I. V. Basistiy, V. Y. Bazhenov, M. S. Soskin, and M. V. Vasnetsov, "Optics of Light Beams With Screw Dislocations," Optics Communications **103**, (5-6), 422-428, (1993).

33 G. Indebetouw, "Optical vortices and their properies," Journal of Modern Optics **40**, (1), 73-87, (1993).

34 F. S. Roux, "Diffractive Lens With a Null in the Center of Its Focal Point," Applied Optics **32**, (22), 4191-4192, (1993).

35 M. W. Beijersbergen, R. P. C. Coerwinkel, M. Kristensen, and J. P. Woerdman, "Helical-Wavefront Laser Beams Produced With a Spiral Phaseplate," Optics Communications **112**, (5-6), 321-327, (1994).

36 C. Paterson, "Diffractive Optical Elements With Spiral Phase Dislocations," Journal of Modern Optics **41**, (4), 757-765, (1994).

37 M. Harris, C. A. Hill, and J. M. Vaughan, "Optical Helices and Spiral Interference Fringes," Optics Communications **106**, (4-6), 161-166, (1994).

38 I. Freund, and N. Shvartsman, "Wave-Field Phase Singularities - the Sign Principle," Physical Review A **50**, (6 Part A), 5164-5172, (1994).

39 C. P. Smith, and R. McDuff, "Charge and Position Detection of Phase Singularities Using Holograms," Optics Communications **114**, (1-2), 37-44, (1995).

40 I. V. Basistiy, M. S. Soskin, and M. V. Vasnetsov, "Optical Wavefront Dislocations and Their Properties," Optics Communications **119**, (5-6), 604-612, (1995).

41 O. V. Angelsky, R. N. Besaha, and I. L. Mokhun, "Appearance of Wave Front Dislocations Under Interference Among Beams With Simple Wave Fronts," Optica Applicata **27**, (4), 273-278, (1997).

42 Z. Jaroszewicz, J. Morales, C. Ramirez, and M. Sypek, "Directional Narrowing of the Diffractive Pattern Through a Combination of Spherical and Spiral Optical Elements Within a Single Aperture," Applied Optics **36**, (31), 8085-8090, (1997).

43 G. F. Brand, "Generation of Millimetre-Wave Beams With Phase Singularities," Journal of Modern Optics **44**, (6), 1243-1248, (1997).

44 M. S. Soskin, V. N. Gorshkov, M. V. Vasnetsov, J. T. Malos, et al., "Topological Charge and Angular Momentum of Light Beams Carrying Optical Vortices," Physical Review A **56**, (5), 4064-4075, (1997).

45 D. L. Fried, and J. L. Vaughn, "Branch cuts in the phase function," Applied Optics **31**, (15), 2865-2882, (1992).

46 M. S. Soskin, and M. V. Vasnetsov, "Nonlinear Singular Optics," Pure & Applied Optics 7, (2), 301-311, (1998).

47 R. Penrose, "The topology of ridge systems," Ann. Hum. Genet.,Lond. **42**, 435-444, (1979).

48 M. Kass, and A. Witkin, "Analyzing oriented patterns," Computer vision, graphics, and image processing **37**, 362-385, (1987).

49 C. F. Shu, and R. C. Jain, "Direct Estimation and Error Analysis For Oriented Patterns," CVGIP-Image Understanding **58**, (3), 383-398, (1993).

50 D. C. Ghiglia, and M. D. Pritt, Two-dimensional phase unwrapping, John Wiley and Sons, New York, 1998.

51 V. V. Kotlar, and V. A. Soifer, "Rotor spatial filter for trhe analysis and synthesis of coherent fields," Optics Communications **89**, 159-163, (1992).

52 E. Abramochkin, and V. Volostnikov, "Rotor Spatial Filter For Analysis and Synthesis of Coherent Fields - Comment," Optics Communications **105**, (5-6), 421-422, (1994).

53 V. V. Kotlar, and V. A. Soifer, "Rely to comment on Rotor Spatial Filter For Analysis and Synthesis of Coherent Fields," Optics Communications **105**, 421-422, (1994).

54 C. Pudney, and M. Robbins, "Surface extraction from 3D images via local energy and ridge tracing," DICTA, (1995), 240--245.

55 E. Peli, "Contrast in complex images," Journal of the Optical Society of America, A **7**, (10), 2032-2040, (1989).

56 A. I. Zayed, Handbook of generalized function transformations, CRC, Boca Raton,

57 D. Hilbert, Grundzuge einer allgemeinen Theorie der linearen Integralgleichungen, 1912.

58 E. C. Titchmarsh, Introduction to the theory of Fourier integrals, Oxford Unversity Press, New York, 1937.

59 P. M. Woodward, Probability and information theory with applications to radar, Pergamon, New York, 1953.

60 J. Dugundji, "Envelopes and pre-envelopes of real waveforms," IRE Trans. Inf. Th. **4**, 53-57, (1958).

61 H. Urkowitz, "Hilbert transforms of bandpass functions," Proceeedings of the IRE **50**, 2143, (1962).

62 E. Bedrosian, "A product theorem for Hilbert transforms," Proceeedings of the IEEE **51**, 868-869, (1963).

63 R. N. Bracewell, The Fourier transform and its applications, McGraw Hill, New York, 1978.

64 M. Takeda, H. Ina, and S. Kobayashi, "Fourier-transform method of fringe-pattern analysis for computer-based topography and interferometry," J. Opt. Soc. Am. **72**, (1), 156-160, (1982).

65 K. A. Nugent, "Interferogram analysis using an accurate fully automatic algorithm," Applied Optics **24**, (18), 3101-3105, (1985).

66 D. J. Bone, H.-A. Bachor, and R. J. Sandeman, "Fringe-pattern analysis using a 2-D Fourier transform," Applied Optics **25**, (10), 1653-1660, (1986).

67 V. I. Vlad, and D. Malacara, "Direct spatial reconstruction of optical phase from phase-modulated images," Progress in Optics, ed. Wolf, E. Progress in Optics, Elsevier Science B.V., 1994) XXXIII: 261-317.

68 N. K. Bose, and K. A. Prabu, "Two-dimensional discrete Hilbert transform and computaional complexity aspects in its implementation," IEEE Transactions on Acoustics, Speech, and Signal Processing **27**, (4), 356-360, (1979).

69 I. Amidor, "Fourier spectrum of radially periodic images," JOSA,A **14**, (4), 816-826, (1997).

70 P. Maragos, and A. C. Bovik, "Image Demodulation Using Multidimensional Energy Separation," Journal of the Optical Society of America A-Optics & Image Science **12**, (9), 1867-1876, (1995).

71 C. F. Shu, and R. C. Jain, "Vector Field Analysis For Oriented Patterns," IEEE Transactions on Pattern Analysis & Machine Intelligence **16**, (9), 946-950, (1994).

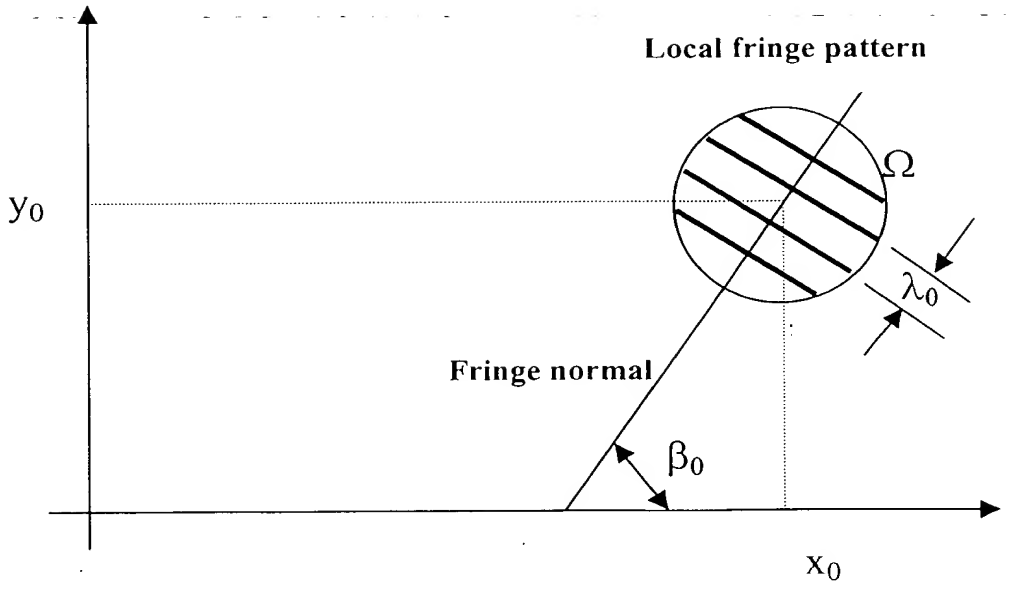
Local fringe pattern
Ω
y_0
λ_0
Fringe normal
β_0
x_0

Fig. 1

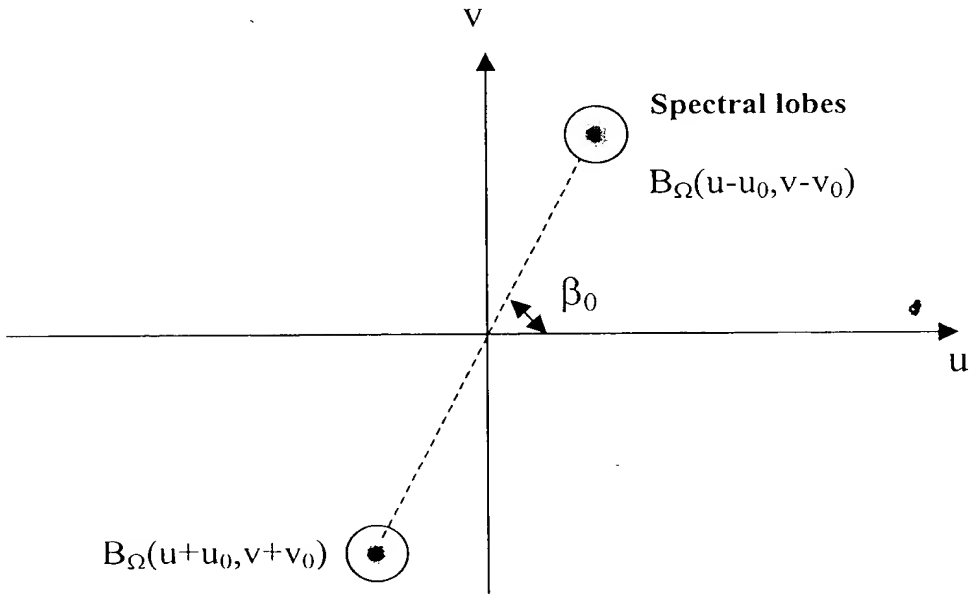
v
Spectral lobes
$B_\Omega(u-u_0,v-v_0)$
β_0
u
$B_\Omega(u+u_0,v+v_0)$

Fig. 2

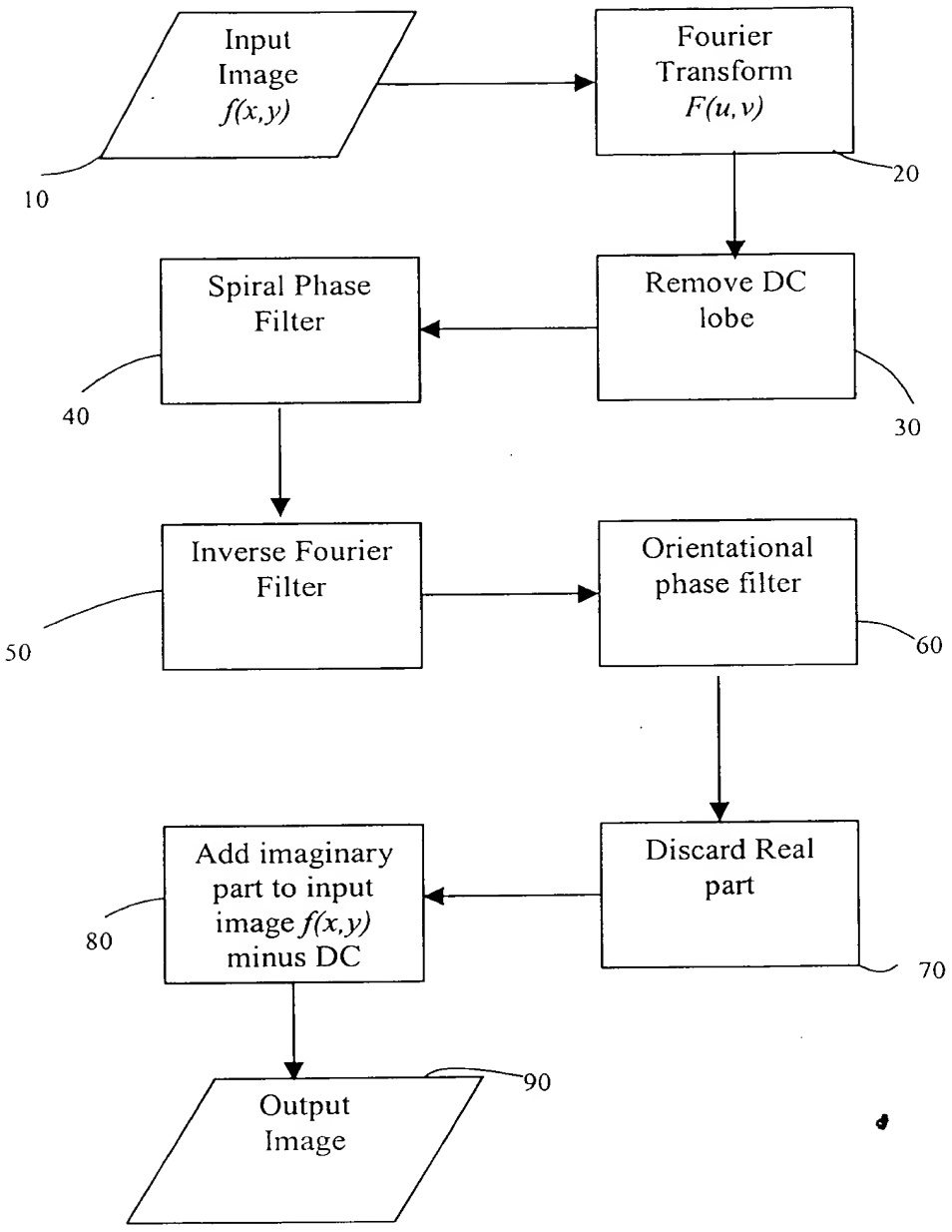
Input Image f(x,y)
10
Fourier Transform F(u,v)
20
Remove DC lobe
30
Spiral Phase Filter
40
Inverse Fourier Filter
50
Orientational phase filter
60
Discard Real part
70
Add imaginary part to input image f(x,y) minus DC
80
Output Image
90

Fig. 3A

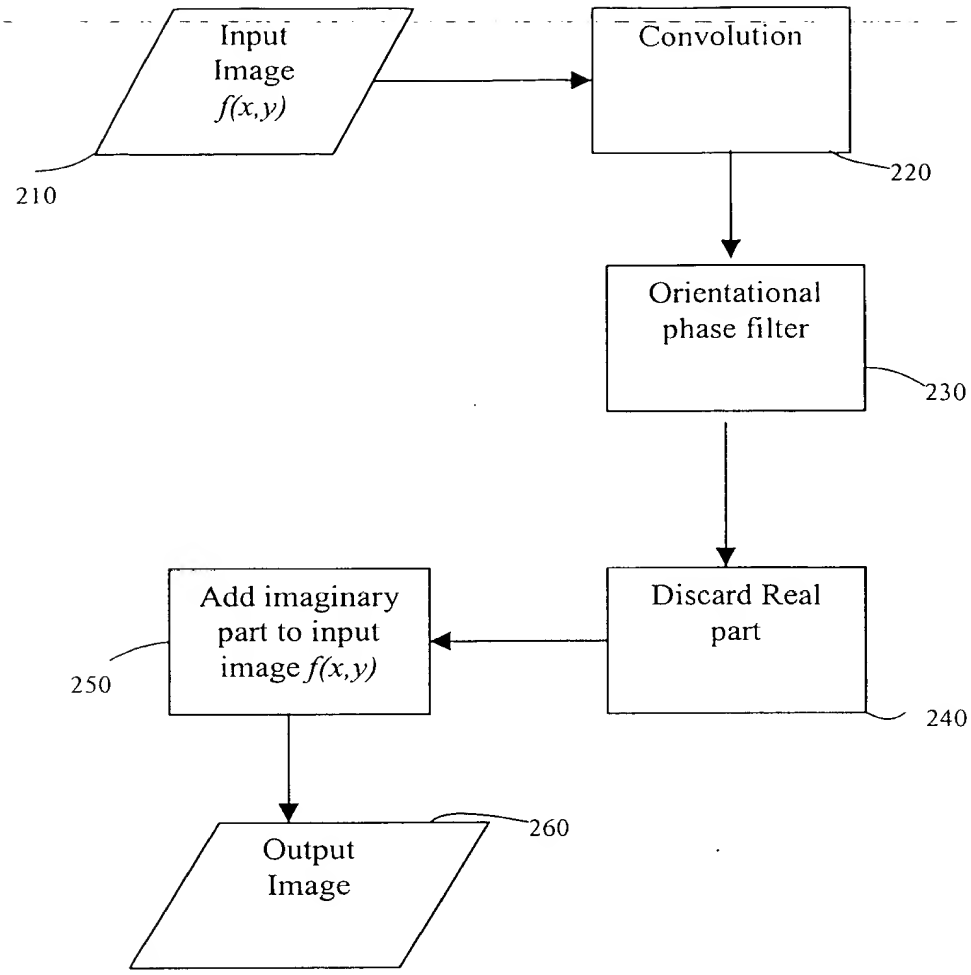
Input Image f(x,y)
210
Convolution
220
Orientational phase filter
230
Discard Real part
240
Add imaginary part to input image f(x,y)
250
Output Image
260

Fig. 3B

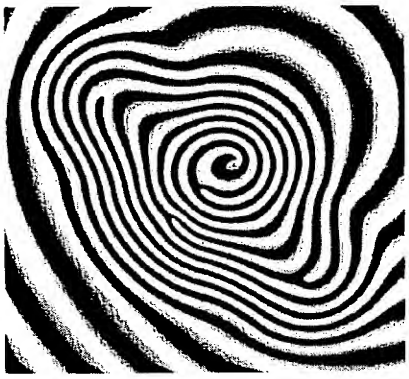

Fig. 4

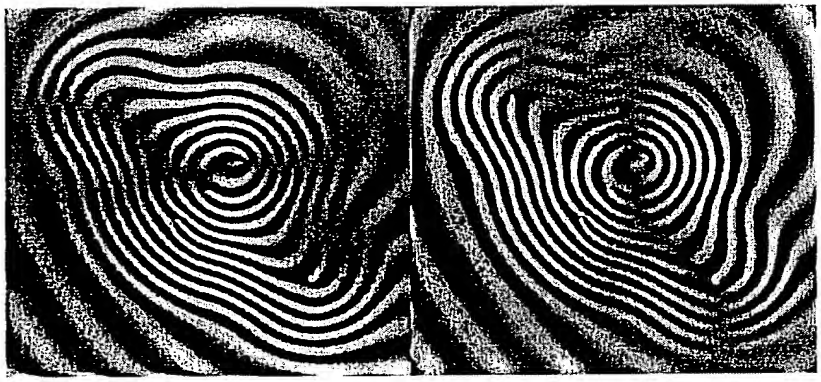

Fig. 5A

Fig. 5B

Fig. 6

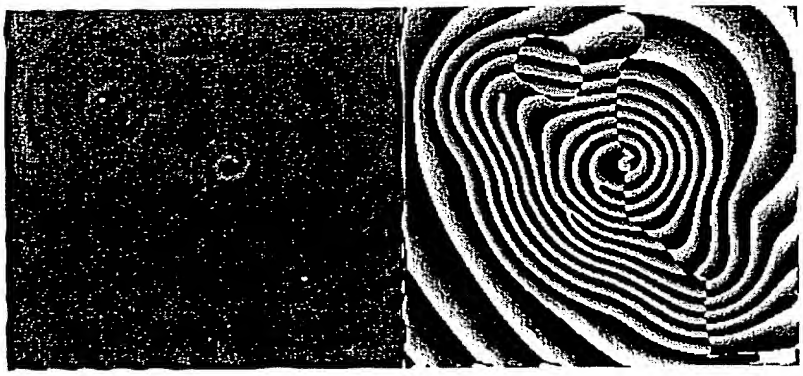

Fig. 7A

Fig. 7B

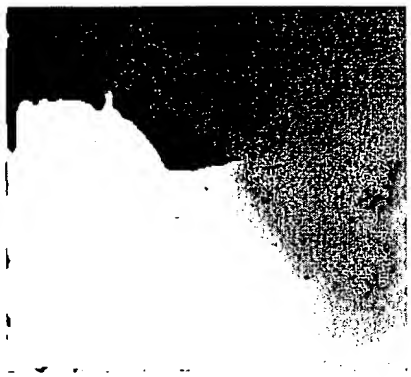

Fig. 8

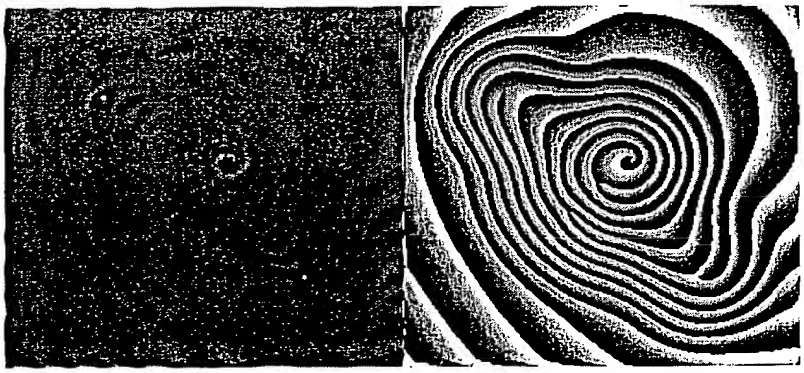

Fig. 9A

Fig. 9B

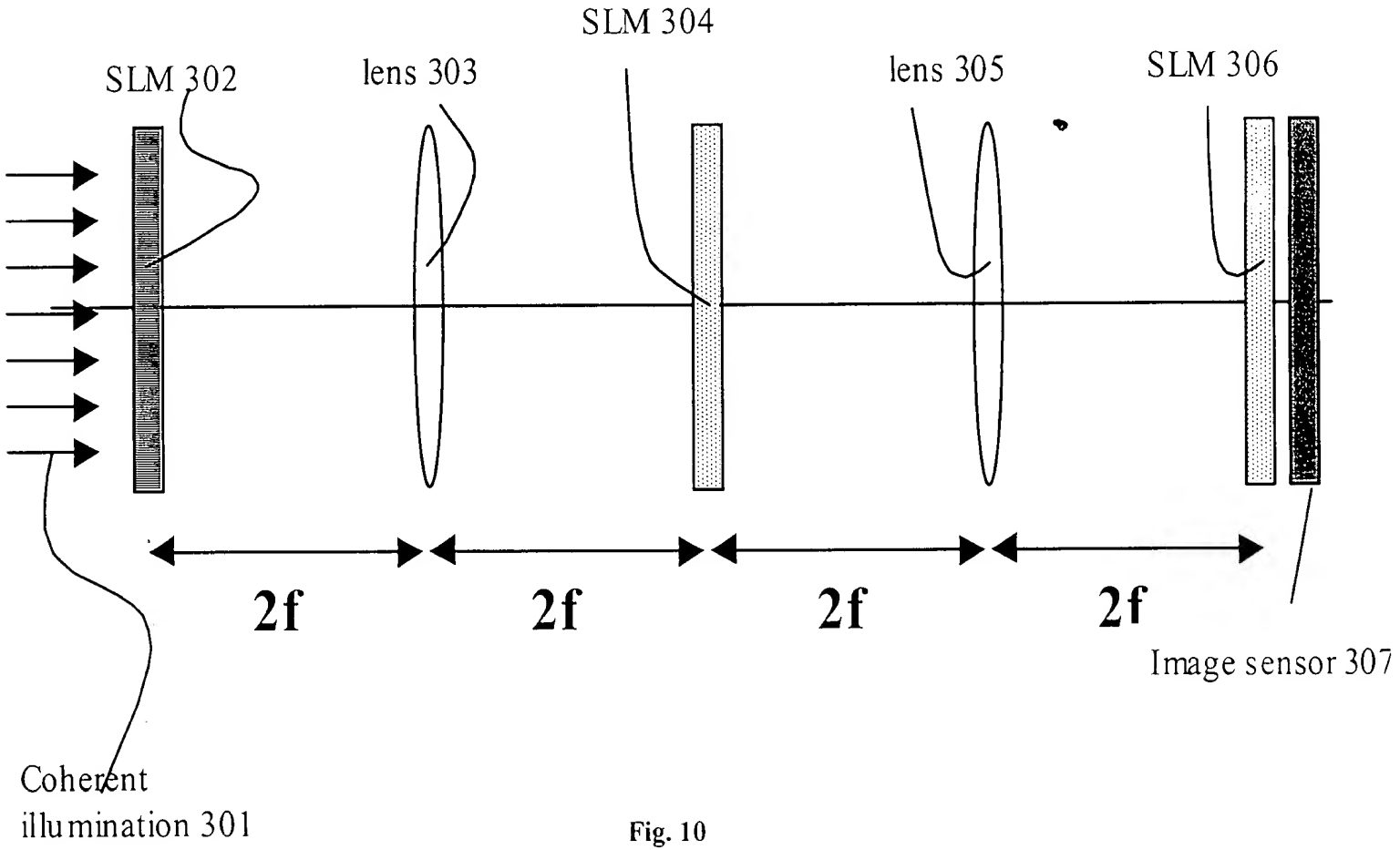
SLM 304
SLM 302
lens 303
lens 305
SLM 306
2f
2f
2f
2f
Image sensor 307
Coherent
illumination 301

Fig. 10

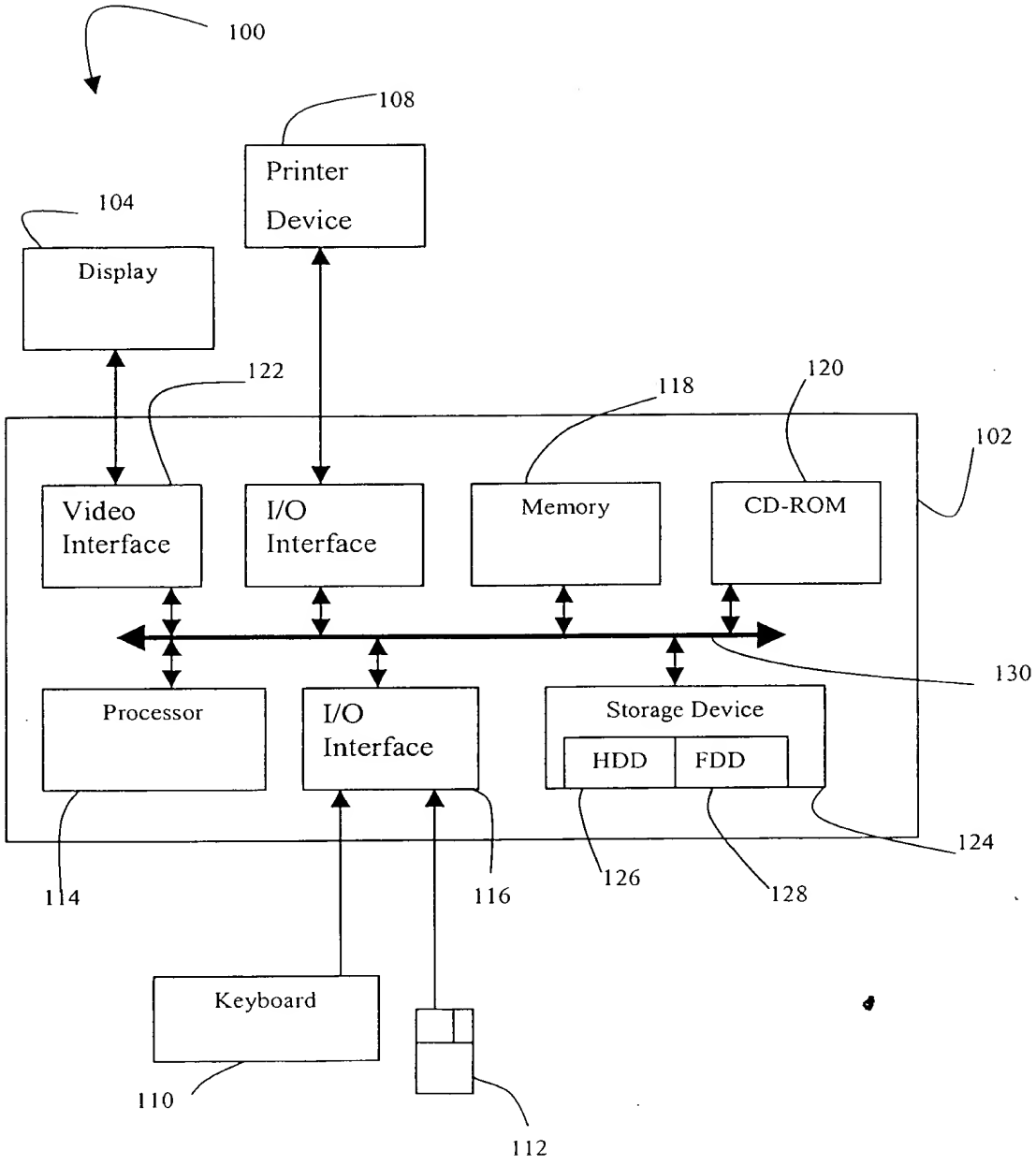
100
108
Printer
Device
104
Display
122
118
120
102
Video
Interface
I/O
Interface
Memory
CD-ROM
130
Processor
I/O
Interface
Storage Device
HDD
FDD
124
114
116
126
128
Keyboard
110
112

Fig. 11